CRB1 gene therapy coming of age: mechanistic insight and rAAV assays on mouse & human retinal organoid models

Buck, T.M.

Chapter 5

CRB1 is required for the recruitment of NOTCH1 and proper recycling by RAB11A+ vesicles in human retinal organoids

Thilo M. Buck, Peter M.J. Quinn, Lucie P. Pellissier, Aat A. Mulder, Aldo Jongejan, Daniëlle, Koot, Hind Almushattat, Christiaan H. Arendzen, Rogier M. Vos, Edward J. Bradley, Christian Freund, Harald M.M. Mikkers, Camiel J.F. Boon, Perry D. Moerland, Frank Baas, Abraham J. Koster, Jacques Neefjes, Ilana Berlin, Carolina R. Jost, Jan Wijnholds.

Submitted

Abstract

Mutations in the *CRB1* gene are a leading cause of monogenetic early-onset blindness in children. Recapitulating human *CRB1* phenotypes in animal models has proven challenging; necessitating the development of alternatives. We have generated human iPSC-derived retinal organoids of patients with retinitis pigmentosa caused by biallelic *CRB1* mutations and evaluated them against autologous gene-corrected hiPSCs and hiPSCs from healthy individuals. We find that patient organoids suffer loss of cell adhesion, photoreceptors and CRB1 & NOTCH1 expression. Using a proximity ligation assay, we show that CRB1 and NOTCH1 can interact on the extracellular domain. *CRB1* patient organoids also feature large EEA1- and WDFY1-positive vesicles, fewer RAB11A+ recycling endosomes and more degradative endolysosomal compartments relative to their normal counterparts. Taken together, our data demonstrate that patient-derived retinal organoids enable modelling of retinal degeneration and highlights the importance of CRB1 in early endosome maturation receptor recycling in the neuroretina.

Introduction

In mammals, the Crumbs (CRB) protein family consists of CRB1, CRB2, and CRB3A, the latter lacking a large extracellular domain [1]. Mutations in the *CRB1* gene are responsible for retinal diseases such as retinitis pigmentosa (RP), Leber congenital amaurosis (LCA) and macular dystrophy [2–6]. Cell adhesion and cell polarity protein complexes at the retinal outer limiting membrane (OLM), such as adherens junctions and CRB complexes play a critical role in the proliferation of retinal progenitor cells (RPCs) [7,8] as well as in cell adhesion [9–11]. The CRB complex is located at the subapical region adjacent to the adherens junctions between RPCs in the developing retina and at the subapical regions of Müller glial cells (MGCs), photoreceptor cells (PRCs), PRCs-PRCs, and PRCs-MGCs [10,12,13]. Retinal cell generation and retinal maturation in the mouse occurs from embryonic day (E) 11 to postnatal day (P) 10. In humans, the same process takes place from fetal gestation week 14 to the first year of life in men [14] and early retinal development can be mimicked in human induced pluripotent stem cell (hiPSC)-derived retinal organoids [12].

We have previously described that the CRB protein levels at the apical membrane in PRCs and MGCs are a major determinant of the severity of the retinal phenotype in $Crb1^{KO}$ and $Crb1^{KO}Crb2^{cKO}$ (cKO, conditional knockout) mice compared to controls [7–11,15,16]. Interestingly, only knocking out *Crb1* [10,11] or expressing a variant *Crb1* (natural occurring $Crb1^{rd8}$) in mice [17] or rat [18,19] did not result in an early developmental phenotype as seen in LCA-*CRB1* patients [2,20], pointing to interspecies differences. Such discrepancy may be due to the restriction of murine Crb1 protein expression to MGCs, while human and non-human-primate CRB1 is expressed in both PRCs and MGCs [12,13,21]. In contrast to CRB1, CRB2 protein is present in PRCs as well as MGCs in both species[9]. Finally, little is known about expression or localization of proteins harbouring disease-causing amino-acid variations in CRB1. Previous mouse and fruit fly studies have identified *Crb* variant-related gain-/loss-of-function phenotypes [22,23]. We showed that the RP *CRB1* patient-derived retinal organoids expressing different variant CRB1 proteins ($CRB1^{M1041T/\ M1041T}$; $CRB1^{Y631C/E995*}$; $CRB1^{M1041T/C948Y}$) have little cell polarity and cell adhesion markers at differentiation day (DD) 180, permitting local displacement of photoreceptor cell columns [12]. Loss of apical polarity has been previously linked to the dysregulation of the endolysosomal system [24–27]. The membrane vesicle trafficking system has been associated with many diseases but, to our knowledge, has not been studied in detail in human retinal organoids.

Numerous reports have previously demonstrated a link between loss of the CRB complex and activation of the Notch signal pathway [7,28,29]. We specifically focused on NOTCH1 because it regulates the retinal progenitor cells (RPCs) population and the differentiation of RPCs into early-born cone PRCs and late-born rod PRCs in mice [30–34]. Additionally, a direct interaction between extracellular domains (ECD) of the Notch-Crb was observed in

fruit fly and zebrafish models. The ECD of Crb in fruit fly or Crumbs2 in zebrafish stabilizes the Notch receptor at the apical membrane [26,35–37]. Furthermore, *Drosophila* Crb mutant protein (crb^{P13A9}) decreases Notch receptor localization at the plasma membrane, increases Notch intracellular domain (ICD) concentrations which actives the Notch pathway, and expands the number of lysosomes in rhabdomeres (a cluster or PRCs & support cells in flies) compared to controls [27].

In the present study, we first gather target genes govering the molecular mechanisms of the *CRB1* LCA-like phenotype in mice. We identify *Wdfy-1*, an overexpressed gene in the *CRB1* LCA-like mouse model, pointing to a misregulation of early endosomes [38]. We follow up on the endolysosomal system in human retinal organoids. First, we generate isogenic controls for patient hiPSCs and validate the evolution of the human RP-*CRB1* phenotype in retinal organoids over time (DD90, 120, 150 and 180). We find a strong decrease of apical CRB1 variant & apical NOTCH1 proteins with a concomitant loss of photoreceptor cells at DD180. We then backtrace how the loss of CRB1 variant proteins appear by investigating the trafficking and degradation of CRB1 proteins. We find that the loss of CRB1 variant protein coincides with a repression of the maturation of early endosomes (EE) shown by an increase of WDFY1 and EEA1 in EE, a reduction of RAB11A+ recycling endosomes, and an increase in degradative endolysosomal compartments in patient organoids. This study suggests that (a) CRB1 is involved in EE/recycling endosome maturation and (b) patients with the common RP *CRB1*-associated mutations ($CRB1^{Met1041Thr}$; $CRB1^{Cys948Tyr}$) have little CRB1 in the neuroretina thus potentially benefiting from a gene supplementation therapy.

Results

Deletion of Crb1 and Crb2 in the developing mouse neuronal retina reveals molecular defect at the endolysosomal system using RNAseq data

To identify the developmental degradative molecular mechanisms in the neural retina lacking CRB1 and CRB2, we first examined the mouse phenotype of $Crb1^{KO}$ ($Crb1^{KO}Crb2^{Flox/Flox}$) and $Crb1^{KO}Crb2^{\Delta RPC}$ conditional knockout (cKO) mice backcrossed into 100% C57BL/JOlaHsd. In agreement with previous findings on mixed genetic background [7], we show in $Crb1^{KO}Crb2^{\Delta RPC}$ mice at embryonic day 15.5 (E15.5), E17.5, postnatal day 1 (P1), 1 month (1M), 3M, 6M and 12M that CRB1 and CRB2 are essential for proper retinal development preventing disturbed retinal layering and loss of retinal function (Figure 1 A-B; Figure S1 and Figure S2). Of note, the 100% C57BL6/JOlaHsd genetic background against the 50% background show a slightly milder retinal phenotype at foci (Figure 1 C; Figure S1). Some regions in the retina mimic the previously described $Crb1^{WT/KO}Crb2^{\Delta RPC}$ cKO retinal phenotype, whereas other regions mimic the more severely affected $Crb1^{KO}Crb2^{\Delta RPC}$ retina on mixed genetic background [7]. The severity of the phenotype was still comparable to the mixed genetic background, considering retinal cell loss measured by retinal thickness (Figure S2 H) and the loss of the retinal response to light flashes measured by ERGs (Figure S2 I-K)

in 1-M-old mice [7]. Previous studies on developing *Crb1*^{KO}*Crb2*$^{\Delta RPC}$ retinas (<P1) on mixed genetic background showed a transiently thicker retina with an increased number and mislocalization of late-born cells (rod PRCs, bipolar cells, MGCs, late-born amacrine cells), increased cell proliferation and apoptosis, dysregulation of the cell cycle, which severely impairs retinal function in adult mice. It has been speculated that CRB1 and CRB2 suppress the cell proliferation of retinal progenitors by regulation of mitogenic signalling pathways such as Notch, YAP and Sonic Hedgehog [7]. We also found an upregulation of mitotic cells (pH3+ cells) at P1 and P5 (Figure 1 F) indicative of an increase in cell proliferation on the 100% C57BL/6JOlaHsd background.

We, therefore, performed RNAseq on mouse neuroretina to gain insights into these developmental changes at the transcriptional level. A comparison between *Crb1*^{KO}*Crb2*$^{\Delta RPC}$ and *Crb1*^{KO} retina, at E15.5, or E17.5, or P1 on 100% C57BL/6JOlaHsd, yielded only subtle persistent changes at the transcriptional level over time (Figure 1 G-I, respectively), despite significant differences in morphology. As internal positive control at E15.5, E17.5 and P1 we used ATP-binding cassette, sub-family D (ALD), member 4 (*Abcd4*), which is substantially upregulated in mouse retina expressing the *Cre* recombinase fused to the *Chx10* promoter, with the *Abcd4* gene immediately adjacent to the *Chx10Cre* locus in the mouse genome. The *Abcd4* expression and other genes were also validated by qPCR at P1 (Figure S2 L).

To further examine potential transcriptional changes at E15.5, we compared *Crb1*^{KO}*Crb2*$^{\Delta RPC}$ mice in 100% C57BL/6JOlaHsd genetic background against wild type C57BL/6JRccHsd mice. In this setting, we observed 40 differentially expressed genes (DEGs) compared to the previously 0 DEGs (E15.5; adj. p-val < 0.01 & log2FC > 1.5. See also Table S4). The *Crb1*^{KO}*Crb2*$^{\Delta RPC}$ mice on C57BL/6JOlaHsd genetic background, due to mutations in the synuclein alpha (*Snca*), multimerin-1 (*Mmrn1*), and *Crb1* gene, do not express *Snca*, *Mmrn1*, or *Crb1* gene transcripts, and express high levels of *Abcd4* due to the adjacent *Chx10Cre* transgene on chromosome 6. We made use of all 4 genes as negative and positive controls in the gene expression profiling, since the mice on C57BL/6JRccHsd genetic background have no mutations in *Snca*, *Mmrn1* or *Crb1* and express low levels of *Abcd4* [39]. Analysis of the E15.5 data revealed upregulated expression of the WD repeat and FYVE domain-containing protein 1 (*Wdfy1*) gene also known as *FYVE domain-containing protein localized to endosomes* (*Fens-1*), which encodes a phosphatidylinositol 3-phosphate binding protein that contains a FYVE zinc finger domain and multiple WD-40 repeat domains (Figure 1 J). These results are in line with the data from *Crb* fruit fly genetics [25–27] that imply changes in the *Crb* endolysosomal system at the OLM. The *CRB1* RP-like morphologic phenotype in mouse, and the surprisingly subtle differences on transcript levels (*Crb1*^{KO}*Crb2*$^{\Delta RPC}$ against wildtype mice) with the *Wdfy1* being upregulated and potential localizing on early

endosomes, prompted us to investigate if major CRB1 variant proteins affect early endosomes in *CRB1* RP-like human patient-derived retinal organoids (Figure 1 K).

Characterization of CRB1 patient retinal organoids

To investigate the disease-state in a human system, we first validated the *CRB1* RP retinal organoid model. We generated isogenic hiPSC controls to exclude that different genetic backgrounds were mediating the *CRB1* patient organoid phenotype. We generated them by homology directed repair (HDR) of the *CRB1*^{M1041T} variant using CRISPR/Cas9 (Figure S3; Table S1). At DD90, all hiPSC lines developed retinal organoids with an outer nuclear layer with PRCs (ONL, OTX2+ nuclei layer) and an inner retina with ganglion cells (BRN3A+ nuclei; Figure 2 A-E; Figure S4 A-C). This indicates that the induction took place for the eyefield development, the optic vesicle regionalization, followed by the retinal neurogenesis. We found a significant decrease in ONL thickness in patient retinal organoids compared to their isogenic controls (Figure 2 F), as well as a decrease in the number of OTX2+ nuclei in the ONL (Figure 2 G) and an increase in the number of PR nuclei above the OLM at DD180 (Figure 2 H). Subsequently, we validated expression of wild type CRB1 and variant CRB1 proteins (encoded by *CRB1*$^{M1041T/\ M1041T}$, *CRB1*$^{M1041T/C948Y}$ or *CRB1*$^{Y631C/E995*}$) by monitoring fluorescence over time using two different antibodies recognizing either an epitope on the short intracellular domain (ICD) of CRB1 or the first EGF-like domains of the ECD. The CRB1-ECD/CRB1-ICD antibodies have a high CRB1-antigen specificity with little background observed on immuno-EM and IHC on human donor cadaveric retinas [13]. Both antibodies indicated a clear CRB1 expression in the isogenic and control organoids at 180 (Figure 2 F-G; Figure S4 D-E). No CRB1-ECD/ICD overlapping signal was found at DD90/DD120 (Figure S4 H-M) which is at the onset of CRB1 expression (DD120) previously found on TEM [12]. Very weak signal was observed at the OLM in the *CRB1* patient lines compared to the isogenic or control retinal organoids at DD180 (Figure 2 F-I; Figure S4 L+M). Thus, the *CRB1* RP organoid model permits comparative protein analysis and is not related to the differences in genetic backgrounds of the control organoids. Also, the reduction of CRB1 variant expression at the OLM suggests that patient-derived gene mutations may alter trafficking of CRB1-containing vesicles to the OLM or the CRB1 turnover at the OLM (cartoon Figure 1 K).

CRB1/NOTCH1-ECD interact and variant CRB1 reduces apical NOTCH1 expression

The retinal thickening seen in *CRB1* LCA-associated patients [2] might be associated with increased cell proliferation during development or a loss of cell adhesion and cell organization. Both has been found in previous *CRB1* LCA mouse studies [7–11,15,16]. An increase in number of retinal cells in patient retinal organoids during development was not found (Figure 2). Also, we found a strong reduction of adhesion markers at DD180 [12]. Interesting candidates bridging loss-of-adhesion with cell proliferation have been NOTCH receptors, especially NOTCH1. For example, mouse *Notch1* was shown as the driving force

behind the developmental shut down by downregulating the Notch pathway activity in RPCs in the mouse neuroretina [40]. *Notch1* is essential in maintaining the RPC population (cycling cells) in the developing retina. Conditional knockdown of *Notch1* restricts the RPC sub-population and confines the differentiation capacity of RPCs mainly to cone photoreceptors [30,33,34,41]. Also, the fruit fly Crb mutant protein (crb^{P13A9}) decreases Notch receptor localization [27].

NOTCH1 was expressed in the RPE at all time points serving as a positive control (Figure 3 A+C-D). We found, as expected, little NOTCH1 expression at the OLM in immature healthy human retinal organoids (DD90. Figure 3 B) or fetal retina (Figure 3 C). In developed retinas (DD180), NOTCH1 expression was almost exclusively limited to MGC-villi at the OLM (co-labelled with CD44-MGC-villi marker and not with the PRC/on-bipolar marker recoverin (Figure 3 E-F). This indicates that apical NOTCH1 expression is linked to the developmental stage in human retinal organoids. *CRB1* patient retinal organoids expressed little NOTCH1 at the OLM (Figure 3 G-I) and more NOTCH1 in the inner retina (Figure 3 G-I asterisks). Recently, a NOTCH-CRB interaction on the ECD was indicated by the proximity ligation assay (PLA) in fruit fly [26]. We observed an interaction of CRB1/NOTCH1-ECD by PLA on human retinal organoids in both patient and control retinal organoids (Figure 3 J-M). The interaction signal in patient retinal organoids was reduced at the OLM and increased in the ONL (Figure 3 J-M). The increase of interaction below the OLM may indicate that the CRB1 variants cannot efficiently traffick from RAB11+ endosomes to OLM or not efficiently recycle in RAB11+ vesicles causing CRB1 variant aggregation or altering the endolysosomes below the OLM.

More autophagy-lysosomal compartments in CRB1 retinal organoids

Loss of CRB increased Notch and Delta endocytosis in fruit fly [42] which increases ARL8-positive lysosomes in rhabdomeres compared to controls in a pre-disease state [26,27]. We next sought to determine what endolysosomal vesicles (size, morphology) are affected by the loss of apical CRB1 on transmission electron microscopy (TEM; Figure 4) and then identified & quantified on light microscopy (Figure 5) at DD180. On TEM, we found few electron-dense degradative compartments/vacuoles in control organoids (Figure 4 A-B; no arrowheads) compared to many in patient organoids (Figure 4 E-G; arrowheads) and, surprisingly, some in the heterozygote gene-corrected organoids (Figure 4 C-D; arrowheads). Additionally, the electron-dense adherens junction / subapical region appeared elongated in some patient organoids (Figure 4 E+G; red arrows indicate adherens junction / subapical regions). Furthermore, some cell disruptions were detected in the $CRB1^{M1041T/C948Y}$ organoids (Figure 4 D; asterisks indicate nuclei above adherens junction) as seen on immunofluorescence (Figure 2 F''+G''+H''). Interestingly, we did not find definitive multivesicular bodies in any of the above specimens, suggesting that photoreceptors and Müller glial cells may not utilise them during the endosomal maturation.

The increase in electron-dense degradative compartments/vacuoles on TEM in patient retinal organoids was then semi-quantified on immunofluorescence signal on DD180 retinal organoids. We hypothesized that CRB1 variant is less efficiently shuttled from the ONL/INL to the OLM aggregating in degradative compartments or alternatively that the turnover of CRB1 variant protein at the OLM is higher. Yet, we found an increase of CRB1 variant in only one patient line (*CRB1*^{Met1041Thr}) in the INL/ONL (Figure S5 I), so indicating little overall aggregation. Also, we observed minimal co-labelling of CRB1 variant with the general endolysosomal marker LAMP1 in the ONL/OLM (Figure S5 A'-H'). We found more lysosomal LAMP1+ vesicles in the ONL but not close to the OLM in patient retinal organoids (Figure S5 K-L). Then, we assessed the co-labelling and expression of the small GTPase lysosome kinesin adaptor ARL8A/B with CRB1 (Figure 5). ARL8A/B is primarily found on late lysosomes [43]. Also, ARL8A/B takes part in the anterograde transport of mature lysosomes to the cell and co-mediates the transport of endocytic cargo to lysosomes [43,44]. Arl8+ lysosomes were previously indicated to accumulate Crb variant proteins in fruit fly [27]. We, however, also found little co-labelling of variant CRB1 with ARL8A/B (Figure 5 A-H). Similar to LAMP1, the area of the total ARL8A/B (lysosome/late endosome) punta was increased in the ONL of patient organoids (Figure 5 K-L), implying accumulation of degradative compartments but not an accumulation of CRB1 variant protein.

We also examined CRB1 variant protein being co-labelled with classical autophagy markers such as the ubiquitin-binding protein adapter p62 and the microtubule-associated proteins 1A/1B light chain 3B (LC3B) in the ONL/OLM. The autophagy cargo adapter p62 can transport substrates to the lysosome that have been tagged, e.g. by LIR (LC3-interacting motif for degradation) [45]. P62 provides an important role for selective autophagy of organelles and ubiquitinated misfolded/damaged proteins (here potentially the CRB1 variant protein). Further, p62 has been linked to selective stress-response-induced autophagy and proteostasis and extensively implicated in selective autophagy [45–47]. We found a strong increase in LC3B and p62 presence in *CRB1* patient retinal organoids in the ONL and at the OLM (Figure 6; Figure S6). The increase may be related to changes in the autophagic flux. We added BafA1 to inhibit acidification of endolysosomes by blocking the vacuole-ATPase (H^+/Ca^{2+} antiporter), which is required for fusion of lysosomes with autophagosomes to form auto-lysosomes, and hence for degradation of proteins targeted to lysosomes. We incubated retinal organoids with BafA1 (500 nM) for 6 hours and extracted the lysate. BafA1 induced a robust block of lysosome-autophagosome fusion on individual organoids (Figure 6 I+J; Figure S6 C+D). We found more autophagosome markers (LC3-II) in *CRB1* patient retinal organoids and a decreased autophagic flux (Figure 6 J+K; Figure S6 G+H) pointing towards a blockage of autophagic vesicle removal. We also found little variant CRB1 expression and co-labelling of CRB1 with p62, LC3B or ARL8A/B. Accordingly, CRB1 variant protein might be either expressed at low levels (see also Figure 2+Figure S4), unstable, degraded in

the ONL/INL with little variant CRB1 reaching the OLM, or reach the OLM but show high turnover due to abnormal vesicle sorting.

Loss of CRB1 reduces the pool of recycling endosomes

To determine where the block of autophagic flux takes place, we investigated the expression of RAB11A. RAB11A is a small GTPase regulating the formation of transport vesicles, recycling endosomes and overall intracellular membrane trafficking [48]. The turnover of CRB and CRB membrane integration is also determined by RAB11 [49] (Figure 1 K). We found a strong signal of RAB11A co-labelling with F-actin in control organoids at the OLM (Figure 7 A+C. Figure S7 A-C). The RAB11A/F-actin co-labelling was strongly reduced in *CRB1* RP patient retinal organoids (Figure 7 B+D. Figure S7 D) with RAB11A yielding 50% less signal at the OLM (Figure 7 P). We further investigated the early endosomal population (EEA1+), late endolysosomal population (RAB7+), retromer-positive recycling compartments (RAB7+, VPS35+), and late endolysosomal population (RAB7+, ARL8A/B+). We found little difference in RAB7 expression between patient and control retinal organoids (Figure 7 E-H+I-L+M. Figure S7 E-H). However, less RAB7 co-labeled with VPS35 (Figure 7 E'''-H'''; Figure S7 E'''-H''') while co-labelling with ARL8A/B increased in patient retinal organoids (Figure 7 E''''-H''''. Figure S7 E''''-H''''). Furthermore, the early endosome population was increased in patient retinal organoids (Figure 7 I'-L'+N. Figure S7 I). Finally, we investigated the WDFY1 protein (also called *FYVE domain-containing protein localized to endosomes* [Fens-1]) expression on retinal organoids, which we found to be upregulated at the transcript level in $Crb1^{KO}Crb2^{\Delta RPC}$ compared to wildtype mouse retina (Figure 1 J). We found little co-labelling with early endosomes in control organoids and cross-validated the WDFY1 antibody with another WDFY1 antibody (Figure S8 A+B). Moreover, WDFY1 does not necessarily have to reside on early endosomes but could instead be located in the cytosol from where it is most likely scrapped by the phospholipid PtdIns(3)P, which is actively recruited by EEA1 [38,50]. We noted that early endosomes in patient organoids expressed more EEA1 (Figure S8 C-H) and co-localized with WDFY1/EEA1 (Figure S8 C'''-H'''), indicating that dysregulated early endosomes may recruit more WDFY1. An increase of WDFY1 fluorescence signal was found in the ONL and OLM (Figure S8 I+J). Interestingly, the isogenic retinal organoids that also potentially express CRB1 variant proteins from one allele (genotype: $CRB1^{M1041T/+}$) had an increase of WDFY1 when compared to the three control lines (expressing wildtype CRB1. Figure S8 I+J). Further research will be needed to determine the function of cytosolic WDFY1 and early endosome bound WDFY1, and if more WDFY1 prime early endosomes for degradation or block the autophagic flux.

Discussion

It is still challenging to predict the progression of the spectrum of *CRB1*-associated retinal dystrophy phenotypes in *CRB1* patients based on the identified genotype variants. A thorough

knowledge on the clinical spectrum, detailed phenotyping, the natural history studies [2,4], are important for optimal counselling and patient selection for interventional studies. Here we address three common RP *CRB1*-associated variants on (a) their protein expression profile in the neuroretina (variant CRB1 being lost) and (b) the loss-of-function of the three CRB1 variants on apical early endosome maturation. Both results have implications for the treatment (e.g. supporting early endosome maturation or *CRB* gene supplementation) and information for patients with one of the *CRB1* variants on understanding the etiology.

We started by investigating *CRB1*-associated disease determinants first at the transcriptional level in mice and subsequently ended at the protein level in a human retinal organoid disease model. We find a strong retinal morphological phenotype in the neuroretina of $Crb1^{KO}Crb2^{\Delta RPC}$ mice with little phenotype seen in $Crb1^{KO}$ (comparable to wildtype mice). But, surprisingly, we find few differences on the transcriptional level in $Crb1^{KO}Crb2^{\Delta RPC}$ against $Crb1^{KO}$ RNAseq data similar to a previous microarray study comparing $Crb2^{\Delta RPC}$ against wildtype mouse retina [29]. However, we do find a strong upregulation of *Wdfy1* in $Crb1^{KO}Crb2^{\Delta RPC}$ compared to wildtype mice. The function of *Wdfy1* is still elusive in many cell types but is linked to early endosomes [38]. We also find an upregulation of apical *WDFY1* protein in *CRB1* patient retinal organoids. Taken together, this indicates that loss of apical CRB1 changes the apical endolysosomal system opening new avenues into rescue biomarkers for *CRB* gene supplementation and *CRB1* gene-editing approaches [51].

Little is still known how different CRB1 variant proteins behave in human neuroretinas. We previously showed that $Crb1^{C249W/-}$ mice (C249W corresponds to the human C250W) traffic and express CRB1 at normal levels at the OLM [23]. Yet, when specific mutant CRB proteins (gene mutations on the central domain of the *Crb* gene) are introduced to a *Crb*-null fruit fly model then the *Crb*-null phenotype is exacerbated, the CRB mutant protein mislocalizes in rhabdomeres and aggregates constituting a gain-of-function phenotype [22]. Interestingly, some fruit fly *Crb* gene mutations (e.g. the Crb^{C749W} gene mutation somewhat comparable to the human $CRB1^{C250W}$ variant) exhibited poor CRB protein expression, but is still able to partially rescue degeneration under light stress when introduced to a *Crb*-null fruit fly. Based on the Pellika and Tepass studies (2017), we initially expected that the three CRB1 variants studied here in patient organoids have a gain-of-function related to CRB1 variant aggregation as found in fruit flies because the mutations are similarly located on the *CRB1* gene affecting the transcription/translation of the CRB1 central protein domain. However, we did find a strong reduction of the CRB1 protein in patient organoids pointing towards a loss-of-function phenotype affecting potentially the turn-over of other apical proteins. We show that this is the case for the NOTCH1 receptor because NOTCH1 potentially stabilized by the here newly discovered CRB1/NOTCH1-ECD physical interaction.

The question remains to determine what controls the CRB1 protein expression, localisation and turn-over rate at the OLM to determine the progression of retinal degeneration in *CRB1*-

associated retinal dystrophy phenotypes in *CRB1* patients. In the present study, we focused on the endolysosomal system because we find an increase of the endosome-associated *Wdfy1* gene expression in $Crb1^{KO}Crb2^{\Delta RPC}$ mice and the degradation-associated proteins on the endolysosomes (ARL8/LAMP1/p62/LC3 puncta) in patient retinal organoids. We paid particular attention to the retromer-positive and early recycling compartments. The retromer complex (SNX1/2, SNX5/6, VPS26, VPS29, and VPS35) on early/late endosomes and the budded off vesicles/recycling endosomes (e.g. RAB11A, TfR1) work in synergy for efficient protein recycling in cells [52], thus are potential essential parameters controlling CRB1 protein turn-over. What is more, the retromer proteins VPS26/VPS35 localize on early and late endosomes in fruit fly photoreceptors, and loss of VPS26 or VPS35 considerably increased degradative compartments [53]. Little has been studied in a human situation but more is already known on the mouse or zebrafish *Crb1* family member *Crb2(a)*. The recycling of CRB2 at the apical membrane is determined by binding of its intracellular domain to VPS35 of the retromer complex on early endosomes [25], a highly conserved 37-aa CRB2-ICD harbouring FERM (4.1, ezrin, radixin, moesin)-PDZ(ERLI) domains shared by the family members CRB1, CRB2, and CRB3A (reviewed in [54]). The CRB protein recycling also depends on RAB11 [49]. The ICD of CRB2A on RAB11A+ recycling endosomes takes part in regulating the cell cycle exit of RPCs and maintaining NOTCH1 at the OLM [55]. RAB11 is known to mediate the release of the early endosomal cargo (*e.g.* NOTCH1, CRB1) to the endocytic recycling compartment when peripheral early endosomes experience a temporary peak in PtdIns(3)P integration on their vesicular membrane [50,56]. Potential poor RAB11A-initiated release in *CRB1* patient retinal organoids may also amass WDFY1 mediated by its FYVE domain binding to PtdIns(3)P [38]. Further assays show that the presence of PtdIns(3)P in a membrane is vital for shifting WDFY1 from a soluble and cytosolic form to an early endosome or vesicle membrane-bound form. The actual function and normal equilibrium of cytosolic versus membrane-bound WDFY1 is not known. In line with this, our data on *CRB1* variant patient retinal organoids have reduced retromer-associated late endosomes (VSP35+/RAB7+), an increase in early endosomes destined for degradation (EEA1+/WDFY1+), a decrease of recycling endosomes (RAB11A+), and a concomitant expansion of degradative endolysosomal compartments (ARL8/LAMP1/LC3-II/p62+). We propose that in *CRB1* patient retinal organoids, the disturbed early endosomes are trafficked to degradative compartments lowering the CRB1 protein expression at the OLM.

Finally, we propose that – given the CRB1 loss-of-function phenotype in patient organoids and the phenotypic rescue from one allele (isogenics) as well as knowing that the amount of CRB correlates to the severity of retinal phenotype seen in *Crb1* mouse models [7–9,13,15,16,57] – few copies of *CRB1* or *CRB2* need to be delivered to the retina of RP *CRB1*-associated patients by recombinant adeno-associated viral vectors to have a therapeutic effect.

Materials and Methods

Mice

Procedures concerning animals were performed with permission of the ethical committee of the Leiden University Medical Center and the animal experimentation committee (DEC) of the Royal Netherlands Academy of Arts and Sciences (KNAW) under permit number NIN 12.105. All mice used were maintained on a 99.9% C57BL/6JOlaHsd genetic background with a 12 h day-night cycle and supplied with food and water *ad libitum*. *Crb1*^{KO} (*Crb1*$^{-/-}$) mice [10] were crossed with a retinal *Crb2*$^{\Delta\mathbf{RPC}}$ (*Crb2*$^{F/F}$Chx10*Cre*$^{Tg/+}$ clone P1E9) mouse strain [58,59] to ablate both *Crb1* and *Crb2* during retinal development from retinal progenitor cells. *Cre* starts to be expressed around E9.5 in the retina [59]. The previously made Chx10*Cre* mice were generated by knocking in *GFP-Cre*-IRES-*AP* cDNA in exon-1 of the *Chx10* gene on a Bacterial Artificial Chromosomes (BAC; -55 kb *Chx10* of ATG to +22 kb off of the polyadenylation sequence) [59]. Interestingly, the last exon of the *Abcd4* gene is only ~7000 bp from the last exon of the *Chx10* gene thus was on the BAC. Others have shown that large BACS containing several genes can lead to overexpression of flanking genes [60,61]. We believe the integration of the cDNA in close proximity to the *Abcd4* gene and being both on the BAC may have led to the overexpression of the *Abcd4* gene in *Crb1*^{KO}*Crb2*$^{\Delta RPC}$ mice. *Crb1*^{KO}*Crb2*$^{\Delta RPC}$ mice were compared to littermate *Crb1*^{KO}*Crb2*$^{F/F}$ mice not expressing *Cre*. C57BL/6JOlaHsd mice have a 365 kb deletion ablating the *Mmrn1* and *Snca* and express low levels of *Abcd4* [39,62]. The C57BL/6J substrain (from the Jackson Laboratory) carries a 5-exon-spanning deletion in the *Nnt* gene but C57BL/6JOlaHsd have a wildtype *Nnt* gene [63]. Analysis of the *Crb1*^{KO}*Crb2*$^{\Delta RPC}$ and *Crb1*^{KO}*Crb2*$^{F/F}$ mice was carried out on males and females. Chromosomal DNA isolation and genotyping were performed as previously described [10,58].

Morphology and retinal thickness measurements on plastic mouse eyes

Eyes were collected of double-knockout and control littermate mice. After enucleation, the eyes were fixed in 4% paraformaldehyde in PBS (25 min) and dehydrated in an ethanol series (30 min each step; 30 % EtOH, 50 % EtOH, 70 % EtOH, 2x 90 % EtOH, 2x 100% EtOH). Then, the eyes were hardened in Technovit, sectioned (3 µm), stained (0.5% Toluidine blue), and mounted (Entellan) as previously described [64]. Consecutive brightfield images were taken. We generated spidergrams of the retinal thickness (ILM-to-OLM) for P14, 1 M and 3M-old-mice by measuring at 0.25, 0.5, 0.75, 1.0, 1.25, 1.5, 1.75, 2.0, 2.25, 2.5, and 2.75 mm distance to the optic nerve head (ONH) as previously described [64].

Electroretinography

Electroretinography's (ERGs) were done in dim light on an Espion E2 (Diagnosys, LLC, MA). 1-month-old (1M) mice were dark-adapted (>12 hours). The mice were anesthetized (100 mg/kg ketamine, 10 mg/kg xylazine, intraperitoneal injection) and the pupils were

dilated (atropine drops, 5 mg/mL). Scotopic flash series: -4, -3 , -2, -1, 0, 1, 1.5, 1.9 log cd s/m² light intensity. Photopic flash series at 30 cd/m² background light: -2, -1, 0, 1, 1.5, 1.9 log cd s/m² light intensity. We first recorded the scotopic ERG, followed by a 10 min light exposure (30 cd s/m² light intensity) and then the photopic ERG.

RNA Sequencing

Sequencing was performed using Life Technologies SOLiD5500 with single-end, 50 bp reads. Two separate runs were performed. Run1 contained n=30 mice; n=5 *Crb1*^{KO}*Crb2*$^{F/F}$ (*Crb1*^{KO}) and n=5 *Crb1*^{KO}*Crb2*$^{\Delta RPC}$ (Tg) per development timepoint of the mouse embryo at E15.5, E17.5 and P1. Run2 contained n=9 mice; n=4 *Crb1*^{KO}*Crb2*$^{\Delta RPC}$ mice (C57BL/6JOlaHsd) and n=5 healthy mice (C57BL/6JRccHsd = wildtype, WT) at E15.5. Reads were aligned against mm10, using the 'whole.transcriptome.frag' workflow with bamgen.mqv.threshold set to 20 (Lifescope v2.5). Counts were obtained using the GTF as supplied by Lifescope (transformation of refGene.txt downloaded from UCSC at 25-06-2014) within this workflow.

Differential expression analysis

The analysis was performed as previously [7]. The two runs were analysed separately. Statistical analyses were performed using the edgeR [65](and limma/voom [66] R/Bioconductor packages. One of the *Crb1*^{KO}*Crb2*$^{\Delta RPCC}$ E15.5 samples in the first run was identified as an outlier and removed from the analysis. Genes with more than one count in five or more samples were retained. Count data were transformed to log2-counts per million (logCPM), normalized by applying the trimmed mean of M-values method [67] and precision weighted using voom [68]. Differential expression was assessed using an empirical Bayes moderated t-test within limma's linear model framework including the precision weights estimated by voom. Resulting p-values were corrected for multiple testing using the Benjamini-Hochberg false discovery rate. Additional gene annotation was retrieved from Ensembl (release 90) using the biomaRt R/Bioconductor package. Analyses were performed using R v3.4.1 and Bioconductor v3.5.

Real-time quantitative PCR

RNA was isolated from 5 controls (*Crb1*^{KO}) and *Crb1*^{KO}*Crb2*$^{\Delta RPC}$ retinas using TRIZOL reagent (Gibco life technologies), according to the manufacturer manual, and after the final precipitation dissolved in RNase-free water. After genomic DNA degradation with RNase-free DNase I (New England Biolabs), 1 µg of total RNA was reverse transcribed into first-strand cDNA with Superscript III Plus RNase H-Reverse Transcriptase (Invitrogen) and 50 ng random hexamer primers, during 50 min at 50ºC in a total volume of 20 µl. To the resulting cDNA sample, 14 µL of 10 mM Tris, 1 mM EDTA was added. From all samples, a 1:20 dilution was made and used for qPCR analysis. For this analysis, primer pairs were designed with a melting temperature of 60–62ºC, giving rise to an amplicon of 80–110 bp. Real-time

qPCR was based on the real-time monitoring of SYBR Green I dye fluorescence on a ABI Prism 7300 Sequence Detection System (Applied Biosystems, Nieuwekerk a/d IJssel, The Netherlands). The PCR conditions were as follows: 12.5 µL SYBR Green PCR 26mastermix (Applied Biosystems), 20 pmol of primers, and 2 µl of the diluted cDNA (ca 3 ng total RNA input). An initial step of 50ºC for 2 min was used for AmpErase incubation followed by 15 min at 95ºC to inactivate AmpErase and to activate the AmpliTaq. Cycling conditions were as follows: melting step at 95ºC for 1 min, annealing at 58ºC for 1 min and elongation at 72ºC, for 40 cycles. At the end of the PCR run, a dissociation curve was determined by ramping the temperature of the sample from 60 to 95ºC while continuously collecting fluorescence data. Non template controls were included for each primer pair to check for any significant levels of contaminants. Values were normalized by the geometric mean of the 3 reference genes hypoxanthine-guanine phosphoribosyltransferase, elongation factor 1-alpha and ribosomal protein S27a.

Data repository

The RNA-Seq data have been deposited in the NCBI Gene Expression.

Cell Culture

We previously described the three male *CRB1* RP-patient human induced pluripotent stem cell (hiPSC) lines (Patient line 1-3: LUMC0116iCRB09, LUMC0117iCRB01, LUMC0128iCRB01) and three control lines (CTRL 1-3: LUMC0004iCTRL10 (hPSC^{reg} name: LUMCi029-B), LUMC0044iCTRL44, LUMC0080iCTRL12; see also Table S3; [12]). HiPSCs were maintained on mTeSR1 or mTeSR Plus on matrigel-coated plates and stored in mFreSR (STEMCELL Techologies) or CryoStor CS10 in liquid nitrogen for long-term storage. The pluripotency status and functional pluripotency was performed for at least 3 clones per line or repaired line (Figure S3 C). HiPSC clones were characterized on pluripotency by triple-staining dissociated single cells with OCT3/4, NANOG, and SSEA4 ($1x10^5$ cells/sample; 1 hr at RT) and analyzed on FACS (Flow cytometer, Miltenyi-Vyb). HiPSCs were also differentiated into the three germlayers (STEMdiff Trilineage differentiation kit, Stem Cell Technologies) and stained on coverslips with the conjugated antibodies Nestin (ectoderm), PAX6 (ectoderm), FOXA2 (endoderm), GATA4 (endoderm), vimentin (mesoderm), CDX2 (mesoderm), Brachyury (mesoderm; blocking solution: 4% NSS/PBS with 0.1% Triton X-100; cells incubated with primary antibodies in 4%NSS/PBS for 1 hr at RT). Figure S3 F-G and see Table S2 antibody concentrations).

CRISPR/Cas9-based gene-repair of the hiPSC lines LUMC0116iCRB09 and LUMC0128iCRB01

The *CRB1* variant c.3122T>C (exon 9) was repaired by CRISPR/Cas9 ribonucleoprotein (RNP) mediated homologous recombination. Sequences of the sgRNA and the repair template (ssODN) are provided below. $1x10^5$ single cells were transfected using

electroporation (Neon System). The CRISPR/Cas9 RNP complex (crRNA:tracrRNA duplex (IDT); 10 pmol of crRNA/tracrRNA pre-annealed (IDT)) and the Cas9 V3 (1 µg; IDT) was transfected. Additionally, the homology directed (HRD) repair template (ssODN; 40 pmol) was added to correct the mutation. For screening of targeted clones, a restriction site is introduced via a silent mutation to avoid re-cutting after HDR (Figure S3 B). $3.6x10^5$ cells in 27 µL were mixed with 6 µL ssODN (13.3 µM) and 3 µL Cas9/RNP complex (3.6 µg Cas9, 36 pmol pre-annealed crRNA:tracrRNA). Then, three times 10 µL ($1.0x10^5$ cells per tube. 30 µL and $3.0x10^5$ cells in total per line) were electroporated (Neon System; Thermo Fisher Scientific; 1100V, 20 ms, 2 pulses), then plated on mTeSR-E8 + CloneR supplement (STEMCELL Technologies) into 12-well plates coated with Synthemax® II-SC substrate (Corning) and placed into an incubator (37ºC, 5% CO_2, 20% O_2). Human iPSCs were seeded as single cells 5-7 days post-electroporation (1000 cells / 10-cm plate). Colonies were picked and gDNA isolated (QuickExtract) 8 days after seeding. Genomic DNA covering the variant region was amplified and targeting was analyzed using Taq1 (NEB; R0149) restriction of the PCR fragment. Successful targeting was confirmed by Sanger sequencing (*CRB1* gene exon 9. Figure S3 D-E).

Cas9 nuclease V3 (IDT #1081058); tracrRNA (IDT #1072532); crRNA (IDT, custom-made).

ssODN:
ACAAGTTTGCAGTCAGTGAATGATGGCACATGGCACGAAGTGACCCTTTCGAT
GACAGACCCACTGTCCCAGACCTCCAGGTGGCAAATGGAAGTGGACA

Sequence of crRNA(s) used: CTGGGACAGTGGGTCTGTCG

Sanger sequencing primers:
Fwd: ACCAGAGAACTCACCAATATCAC
Rev: CAATAGCTCTGTCTCCCACATAA

Retinal Organoid Differentiation

The differentiation of the hiPSCs started at differentiation day (DD) 0 with floating single-cell hiPSCs that were self-aggregated to embryoid bodies in 10 µM (±)blebbistatin in mTeSR1 or mTeSR Plus medium (STEMCELL Technologies) on 1% agarose-coated (non-adhesive) plates overnight. The media was gradually changed from mTeSR to the Neural Induction Medium (NIM-1) over three days (mTeSR1/NIM-1: day 0, 1:0, day 1, 3:1; day 2, 1:1, day 3, 0:1). NIM-1 consists of DMEM/F12 supplemented with 1xN2 supplement, 1x Minimum Essential Media Non-Essential Amino Acids (MEM NEAAs) and 2 µg/mL Heparin (Sigma. See also [12]). The medium was changed every day until DD7. The embryoid bodies were plated at an approximate density of 20 aggregates per cm^2 onto Matrigel-coated wells on DD7 and lifted on DD22/28. NIM-1 was replaced every other day from DD7 to DD16, from DD16 medium was replaced each day with Neural induction

medium 2 (NIM-2). NIM-2: 1x B27 or NeuroCult SM1 without Vitamin A, 1x NEAA and 1x antibiotic-antimycotic in DMEM/F12(3:1). Subsequently, the lifted organoids were dislodged and kept in floating culture with NIM-2 on agarose-coated plates. At DD33 forebrain organoids were removed with a truncated P200 pipet tip. Medium was replaced three times a week from DD41 onwards. The medium was changed to Retinal Lamination Medium 1 (RLM-1) at DD42. RLM-1: 10% FBS, 1x B27 without Vitamin A (Gibco) or NeuroCult™ SM1 without Vitamin A (Stem Cell Technologies), 1x NEAA, 1x antibiotic-antimycotic, and 100 µM taurine in DMEM/F12(3:1). The RLM-1 was supplemented with 1 µM retinoic acid from DD49 to DD98. The long-term culture medium from DD98 onwards was Retinal Lamination Medium-2 (RLM-2) with low amounts of growth factors (N2 supplement instead of B27). RLM-2: 10% FBS, 1x N2, 1x NEAA, 1x antibiotic-antimycotic, and 100 µM taurine in DMEM/F12(3:1) 0.5 µM retinoic acid.

Fetal human retinal tissue

The use and collection of the material were approved by the Medical Ethics Committee of the Leiden University Medical Center (P08.087). Patient anonymity was strictly maintained. All tissue samples were handled in a coded fashion, according to Dutch national ethical guidelines (Code for Proper Secondary Use of Human Tissue, Dutch Federation of Medical Scientific Societies).

Fixation, sectioning and immunohistochemical staining

Retinal organoids were collected at the time points of differentiation day(DD)90, 120, 150, and 180. Prior to fixation, the organoids were washed shortly in PBS and then incubated for 30 minutes in 4% paraformaldehyde in PBS. Subsequently, the organoids were dehydrated in 15% sucrose in PBS (30 min) and 30% sucrose in PBS (30 min). After that, the retinal organoids were orientated and embedded in OCT Tissue-Tek cryo-embedding media. Finally, they were frozen on dry-ice and stored at -20°C. The retinal organoids were sectioned at 7 µm using a Leica CM1900 cryostat (Leica Microsystems) and after 1 hour of airdrying stored at -20°C. The slides were rehydrated in PBS, blocked (1 hour. 0.1% BSA 0.04% Triton-X in PBS), stained with the primary antibody (in 0.1% BSA 0.04% Triton-X in PBS) overnight at 4°C or 3 hours at room temperature, washed three times in PBS (3x10 min), stained with the secondary antibody (1 hour), washed three times in PBS (3x10 min), and mounted with Vectashield® Vibrance® HardSet antifade mounting media containing DAPI (Vector Laboratories). For antibodies and dilutions see Table S2. A Leica TCS SP8 confocal microscope was used for image acquisition. Image analysis was done in Leica Application Suite X (Leica, LAS X), Fiji ImageJ, and Adobe Photoshop CC2018.

Fluorescence semi-quantification in ROIs

All organoids (7-µm sectioned) imaged for fluorescence semi-quantification were stained (see Table S2) with the same antibody mix at the same time, imaged in one confocal

microscopy session, and included a negative control (no primary antibody added). At least six different organoids (generally 10-12) per line on generally three glass slides were analyzed per immunofluorescence staining. Several experiments were stained twice and analyzed twice showing overall high robustness of outcome parameters. The semi-quantification of CRB1 protein expression was done in triplicates with different secondary antibodies and incubation times (overnight at +4°C or 3 hours at RT) showing a strong reduction in patient organoids in all conditions. The analysis was done blinded. A 8-bit gray-scale raw image file was loaded into ImageJ. We manually defined three ROIs in the retina: ROI1, OLM (±2.5 µm of OLM); ROI2, ONL (dense bright DAPI+ nuclei layer or OTX2+ nuclei layer below the ROI 1), ROI3, OPL/INL (nuclei layer below the ROI2 of spanning the neuroretina maximally 50 µm below ROI2). First, the mean gray value (MGV) per ROI was analysed. Then, we measured on each ROI the average particle size (area), the number of particles (counts), and the average intensity per spot (value between 0-255) using the ImageJ function "Analyze Particles". We normalized the values to: counts per 100 µm² and the area of all spot sizes per ROI area (%).

Isolation of protein lysates and immunoblotting

Retinal organoids were collected at DD180. The RPE (dark parts) were dissected off with surgical scissors. Single neuroretinas were washed in cold 1xPBS and then lysed in cold RIPA buffer (#R0278, Sigma) including the protease inhibitor cocktail (cOmplete, #11836153001, Roche). The single neuroretinas were mechanical disrupted by pipetting and incubated on ice for 2 hours. Then, the neuroretinas were vortexed and then sonicated in a pre-cooled +4^{0}C water bath (Diagenode Biorupter Pico; Program: 15 sec ON, 30 sec OFF. 4 cycles; vortexed between 1st and 2nd cycle). The samples were then spun down (16000xg, 10 min, +4°C) and the supernatant was collected in a new pre-cooled tube. The protein concentration was measured by the Bradford assay (BCA Protein Assay Kit; ThermoFisher, #23227). The protein was then diluted to 1x Laemmli buffer with DTT (Bio-Rad, #1610737. Buffer: 0.12 M Tris-HCl, pH 6.8, 4% SDS, 20% glycerol, 10 mM DTT), boiled for 5 min (+95°C), and stored at -80°C. The protein lysates (20 µg per organoid per lane) were separated on a 4-20% SDS gel (Bio-Rad, #4561094) and transferred on PVDF (Bio-Rad Turbo transfer system. Protocol: mixed-molecular weight). The blots were blocked in 5% non-fatty milk in 1xPBS 0.1% Tween-20 (PBST; RT, 1 hour), incubated with the primary antibody (see Table S4 for concentrations; 5% milk in PBST), washed, incubated with the HPR-conjugated-antibody (RT, 1 hour 5% milk in PBST), and washed again. The signal was generated in ECL substrate (Bio-Rad, #1705061) and the chemiluminescence was imaged at three different exposure times (ChemiDoc MP Imaging System, Bio-Rad). The band intensity was measured (ImageJ, Gel analyzer) and averaged from three exposure times. Quantification was relative to GAPDH.

Transmission electron microscopy

Samples were washed in 1xPBS and then fixed in 1.5% glutaraldehyde in 0.1M cacodylate buffer at room temperature for 1 hour, stored in 0.5% PFA in 0.1M PHEM storage buffer until further processing. Samples were rinsed three times in 0.1 M cacodylate buffer and post-fixed in 1%OsO_4/1.5% potassium ferricyanide in 0.1M cacodylate buffer (1 hour on ice). Samples were rinsed again in 0.1M cacodylate buffer three times, and dehydrated in a series of ethanol, followed by a series of propylene oxide with EPON (LX112, Ladd research industries) and finally a step in 100% EPON. Organoids were put in a mould, those were filled up with EPON and polymerized at 70°C over two days. Ultrathin sections (90 nm) were created on a Reichert Ultracut S (Leica Microsystems) and after staining with uranylacetate and lead citrate, examined on an electron microscope (Microscope: FEI Tecnai T12 Twin Fei Company, Eindhoven, The Netherlands; Camera: OneView, Gatan) operating at 120 kV. Overlapping images were collected and stitched together into separate images as previously described [69].

Conjugation of NOTCH1 and CRB1 antibody to plus and minus oligonucleotide probes

We used the Duolink probemaker set (Sigma-Aldrich) to conjugate two same-species antibodies (mouse anti-NOTCH1 and mouse anti-CRB1 extracellular domain antibodies) to the plus or minus oligonucleotide probes as described in the protocol. In short: 20 µL of the primary antibody was mixed with 2 µL of the conjugation buffer. Subsequently, the antibodies were added to the Duolink In Situ Probemaker plus and minus vials for overnight incubation at room temperature. The next day, the stop reagent was added (incubation: 30 minutes, at RT), the storage solution was added and stored at +4°C.

Proximity ligation assay

For the proximity ligation assay the Duolink In Situ Detection Reagents kit green (Sigma-Aldrich) was used. Slides with sliced organoids were washed, and the tissue slices were circled with a hydrophobic pen. Slides were blocked with one drop of blocking solution from the Duolink PLA probe set per tissue slice and incubated for 1 hour at 37 °C in a humidity chamber. Blocking buffer was tapped of and the conjugated antibodies diluted in PLA probe diluent from the PLA probe kit were added for an overnight incubation at 4°C. After that the slides were washed twice in PLA wash buffer A (Sigma-Aldrich) for five minutes. For the ligation step the slides were incubated for 30 minutes at 37°C with ligase enzyme diluted (1:40) in 1x ligation buffer and were washed twice in wash buffer A again. Finally, the polymerase enzyme was diluted (1:80) in 1x amplification buffer and added to the slides and the slides were incubated in a humidity chamber (37 °C, 100 minutes). To one of the slides diluted amplification buffer was added without the polymerase, serving as a negative control. Subsequently, the slides were washed twice for 10 minutes in PLA wash buffer B and after that once for 1 minute in 0.01x wash buffer B. Wash buffer was tapped off and slides were

mounted by adding 5 µL of Duolink In Situ Mounting Medium with DAPI with a 20µl pipet with truncated tip. Images were obtained using a Leica TCS SP8 confocal microscope.

Statistical analysis

The organoids were acquired from two or more differentiations and we aimed to obtain 3 images per organoid. Each image was analyzed on retinal length, thickness, total cells and total positive retinal cell population markers with ImageJ. Data were normalized per 100 µm retinal length. For statistical analysis GraphPad Prism version 8 (GraphPad Software) was used. Shown values are expressed as mean ± Standard error of the mean (SEM). Quantifications were tested for normality and if normally distributed unpaired T-tests assuming equal variance were used to compare patient and control lines. Measurements that did not show a normal distribution were tested with a Mann-Whitney test. Significance is indicated in graphs as $p<0.05$ (*), $p<0.01$ (**), and $p<0.001$ (***).

Author contribution

Conceptualization: TMB, PMJQ, LPP, JW. Methodology retinal organoids and mouse morphology: TMB, PMJQ, LPP, AAM, DK. Generation hiPSC lines (patient) & repair (isogenic controls) and hiPSC characterization: CA, CF, HMM. Methodology/software/formal analysis/data curation of RNAseq data set: AJ, AvK, FB, PMJQ, JW. Formal analysis retinal organoids and mouse morphology: TMB, PMJQ, LPP. Investigation: TMB, PMJQ, LPP, JW. Writing – Original Draft: TMB and JW. Writing – Review & Editing: all authors. Visualization: TMB, PMJQ, LPP, JW. Resources: IB, JJCN. Supervision: JW. Funding acquisition: JW.

Acknowledgments

We thank Marco Heuvelman and Yacintha van Doorn for their experimental work and the Wijnholds lab for their advice on experiments and reviewing the manuscript. We thank Annelies Boonzaier-van der Laan & Lennard M. Voortman for the technical assistance on microscopy & image analysis.

Funding

The Netherlands Organization for Health Research and Development (ZonMw grant 43200004, to JW), research grant MDBR-19-131-CRB1 from the University of Pennsylvania Orphan Disease Center in partnership with the Curing Retinal Blindness Foundation (to JW), research grant CRBF 2016-Aug-02 (to JW), and the Dutch blindness funds (Uitzicht 2015-22 to JW, Uitzicht 2020-01 to TMB and JW): Rotterdamse Stichting Blindenbelangen, OogFonds, Stichting Blindenhulp, Stichting Retina Fonds, Landelijke Stichting voor Blinden en Slechtzienden.

Conflict of interest statement

The authors declare that the research was conducted without any commercial or financial relationship that could be construed as a potential conflict of interest. The LUMC is the holder of patent number PCT/NL2014/050549, which describes the potential clinical use of CRB2; JW and LPP are listed as co-inventor of this patent, and JW is an employee of the LUMC.

REFERENCES

1. Quinn, P.M.; Pellissier, L.P.; Wijnholds, J. The CRB1 complex: Following the trail of Crumbs to a feasible gene therapy strategy. *Front. Neurosci.* **2017**, *11*, 175.
2. Talib, M.; van Schooneveld, M.J.; van Genderen, M.M.; Wijnholds, J.; Florijn, R.J.; ten Brink, J.B.; Schalij-Delfos, N.E.; Dagnelie, G.; Cremers, F.P.M.; Wolterbeek, R.; et al. Genotypic and Phenotypic Characteristics of CRB1-Associated Retinal Dystrophies: A Long-Term Follow-up Study. *Ophthalmology* **2017**, *124*, 884–895.
3. den Hollander, A I.; Heckenlively, J.R.; van den Born, L.I.; de Kok, Y.J.; van der Velde-Visser, S.D.; Kellner, U.; Jurklies, B.; van Schooneveld, M.J.; Blankenagel, A; Rohrschneider, K.; et al. Leber congenital amaurosis and retinitis pigmentosa with Coats-like exudative vasculopathy are associated with mutations in the crumbs homologue 1 (CRB1) gene. *Am. J. Hum. Genet.* **2001**, *69*, 198–203.
4. Nguyen, X.-T.-A.; Talib, M.; van Schooneveld, M.J.; Wijnholds, J.; van Genderen, M.M.; Schalij-Delfos, N.E.; Klaver, C.C.W.; Talsma, H.E.; Fiocco, M.; Florijn, R.J.; et al. CRB1-associated retinal dystrophies: a prospective natural history study in anticipation of future clinical trials. *Am. J. Ophthalmol.* **2021**.
5. Khan, K.N.; Robson, A.; Mahroo, O.A.R.; Arno, G.; Inglehearn, C.F.; Armengol, M.; Waseem, N.; Holder, G.E.; Carss, K.J.; Raymond, L.F.; et al. A clinical and molecular characterisation of CRB1-associated maculopathy. *Eur. J. Hum. Genet.* **2018**, *26*, 687–694.
6. Tsang, S.H.; Burke, T.; Oll, M.; Yzer, S.; Lee, W.; Xie, Y.A. (Angela); Allikmets, R. Whole Exome Sequencing Identifies CRB1 Defect in an Unusual Maculopathy Phenotype. *Ophthalmology* **2014**, *121*, 1–10.
7. Pellissier, L.P.; Alves, C.H.; Quinn, P.M.; Vos, R.M.; Tanimoto, N.; Lundvig, D.M.S.; Dudok, J.J.; Hooibrink, B.; Richard, F.; Beck, S.C.; et al. Targeted ablation of CRB1 and CRB2 in retinal progenitor cells mimics Leber congenital amaurosis. *PLoS Genet* **2013**, *9*, e1003976.
8. Alves, C.H.; Pellissier, L.P.; Vos, R.M.; Garcia Garrido, M.; Sothilingam, V.; Seide, C.; Beck, S.C.; Klooster, J.; Furukawa, T.; Flannery, J.G.; et al. Targeted ablation of Crb2 in photoreceptor cells induces retinitis pigmentosa. *Hum. Mol. Genet.* **2014**, *23*, 3384–3401.
9. Quinn, P.M.; Mulder, A.A.; Henrique Alves, C.; Desrosiers, M.; de Vries, S.I.; Klooster, J.; Dalkara, D.; Koster, A.J.; Jost, C.R.; Wijnholds, J. Loss of CRB2 in Müller glial cells modifies a CRB1-associated retinitis pigmentosa phenotype into a Leber congenital amaurosis phenotype. *Hum. Mol. Genet.* **2019**, *28*, 105–123.
10. van de Pavert, S.A.; Kantardzhieva, A.; Malysheva, A.; Meuleman, J.; Versteeg, I.; Levelt, C.; Klooster, J.; Geiger, S.; Seeliger, M.W.; Rashbass, P.; et al. Crumbs homologue 1 is required for maintenance of photoreceptor cell polarization and adhesion during light exposure. *J. Cell Sci.* **2004**, *117*, 4169–4177.
11. van de Pavert, S.A.; Sanz, A.S.; Aartsen, W.M.; Vos, R.M.; Versteeg, I.; Beck, S.C.; Klooster, J.; Seeliger, M.W.; Wijnholds, J. Crb1 is a determinant of retinal apical Müller glia cell features. *Glia* **2007**, *55*, 1486–1497.
12. Quinn, P.M.; Buck, T.M.; Mulder, A.A.; Ohonin, C.; Alves, C.H.; Vos, R.M.; Bialecka, M.; van Herwaarden, T.; van Dijk, E.H.C.C.; Talib, M.; et al. Human iPSC-Derived Retinas Recapitulate the Fetal CRB1 CRB2 Complex Formation and Demonstrate that Photoreceptors and Müller Glia Are Targets of AAV5. *Stem Cell Reports* **2019**, *12*, 906–919.
13. Pellissier, L.P.; Lundvig, D.M.S.; Tanimoto, N.; Klooster, J.; Vos, R.M.; Richard, F.; Sothilingam, V.; Garcia Garrido, M.; Le Bivic, A.; Seeliger, M.W.; et al. CRB2 acts as a modifying factor of CRB1-related retinal dystrophies in mice. *Hum. Mol. Genet.* **2014**, *23*, 3759–3771.

14. Quinn, P.M.J.; Wijnholds, J. Retinogenesis of the human fetal retina: An apical polarity perspective. *Genes (Basel)* **2019**, *10*, 987.
15. Buck, T.M.; Vos, R.M.; Alves, C.H.; Wijnholds, J. AAV-CRB2 protects against vision loss in an inducible CRB1 retinitis pigmentosa mouse model. *Mol. Ther. - Methods Clin. Dev.* **2021**, *20*.
16. Quinn, P.M.; Alves, C.H.; Klooster, J.; Wijnholds, J. CRB2 in immature photoreceptors determines the superior-inferior symmetry of the developing retina to maintain retinal structure and function. *Hum. Mol. Genet.* **2018**, *27*, 3137–3153.
17. Mehalow, A.K.; Kameya, S.; Smith, R.S.; Hawes, N.L.; Denegre, J.M.; Young, J. a; Bechtold, L.; Haider, N.B.; Tepass, U.; Heckenlively, J.R.; et al. CRB1 is essential for external limiting membrane integrity and photoreceptor morphogenesis in the mammalian retina. *Hum. Mol. Genet.* **2003**, *12*, 2179–89.
18. Boon, N.; Henrique Alves, C.; Mulder, A.A.; Andriessen, C.A.; Buck, T.M.; Quinn, P.M.J.; Vos, R.M.; Koster, A.J.; Jost, C.R.; Wijnholds, J. Defining phenotype, tropism, and retinal gene therapy using adeno-associated viral vectors (AAVs) in new-born brown norway rats with a spontaneous mutation in CRB1. *Int. J. Mol. Sci.* **2021**, *22*, 3563.
19. Zhao, M.; Andrieu-Soler, C.; Kowalczuk, L.; Cortés, M.P.; Berdugo, M.; Dernigoghossian, M.; Halili, F.; Jeanny, J.C.; Goldenberg, B.; Savoldelli, M.; et al. A new CRB1 rat mutation links Müller glial cells to retinal telangiectasia. *J. Neurosci.* **2015**, *35*, 6093–6106.
20. Motta, F.L.; Salles, M.V.; Costa, K.A.; Filippelli-Silva, R.; Martin, R.P.; Sallum, J.M.F. The correlation between CRB1 variants and the clinical severity of Brazilian patients with different inherited retinal dystrophy phenotypes. *Sci. Reports 2017 71* **2017**, *7*, 1–9.
21. van Rossum, A.G.S.H.; Aartsen, W.M.; Meuleman, J.; Klooster, J.; Malysheva, A.; Versteeg, I.; Arsanto, J.-P.P.; Le Bivic, A.A.; Wijnholds, J. Pals1/Mpp5 is required for correct localization of Crb1 at the subapical region in polarized Müller glia cells. *Hum. Mol. Genet.* **2006**, *15*, 2659–2672.
22. Pellikka, M.; Tepass, U. Unique cell biological profiles of retinal disease-causing missense mutations in the polarity protein Crumbs. *J. Cell Sci.* **2017**, *130*, 2147–2158.
23. van de Pavert, S.A.; Meuleman, J.; Malysheva, A.; Aartsen, W.M.; Versteeg, I.; Tonagel, F.; Kamphuis, W.; McCabe, C.J.; Seeliger, M.W.; Wijnholds, J. A single amino acid substitution (Cys249Trp) in Crb1 causes retinal degeneration and deregulates expression of pituitary tumor transforming gene Pttg1. *J. Neurosci.* **2007**, *27*, 564–573.
24. Zhou, B.; Wu, Y.; Lin, X. Retromer regulates apical-basal polarity through recycling crumbs. *Dev. Biol.* **2011**, *360*, 87–95.
25. Pocha, S.M.; Wassmer, T.; Niehage, C.; Hoflack, B.; Knust, E. Retromer Controls Epithelial Cell Polarity by Trafficking the Apical Determinant Crumbs. *Curr. Biol.* **2011**, *21*, 1111–1117.
26. Lattner, J.; Leng, W.; Knust, E.; Brankatschk, M.; Flores-Benitez, D. Crumbs organizes the transport machinery by regulating apical levels of pi (4,5)p2 in drosophila. *Elife* **2019**, *8*.
27. Kraut, R.S.; Knust, E. Changes in endolysosomal organization define a pre-degenerative state in the crumbs mutant Drosophila retina. *PLoS One* **2019**, *14*, e0220220.
28. Thompson, B.J.; Pichaud, F.; Röper, K. Sticking together the Crumbs - an unexpected function for an old friend. *Nat. Rev. Mol. Cell Biol.* **2013**, *14*, 307–14.
29. Alves, C.H.; Bossers, K.; Vos, R.M.; Essing, A.H.W.; Swagemakers, S.; van der Spek, P.J.; Verhaagen, J.; Wijnholds, J. Microarray and morphological analysis of early postnatal CRB2 mutant retinas on a pure C57BL/6J genetic background. *PLoS One* **2013**, *8*, e82532.
30. Chen, X.; Emerson, M.M. Notch signaling represses cone photoreceptor formation through the regulation of retinal progenitor cell states. *Sci. Reports 2021 111* **2021**, *11*, 1–18.
31. Mills, E.A.; Goldman, D. The Regulation of Notch Signaling in Retinal Development and Regeneration. *Curr. Pathobiol. Rep.* **2017**, *5*, 323–331.
32. Mizeracka, K.; Demaso, C.R.; Cepko, C.L. Notch1 is required in newly postmitotic cells to inhibit the rod photoreceptor fate. *Development* **2013**, *140*, 3188–3197.

33. Jadhav, A.P.; Cho, S.-H.; Cepko, C.L. Notch activity permits retinal cells to progress through multiple progenitor states and acquire a stem cell property. *Proc. Natl. Acad. Sci.* **2006**, *103*, 18998–19003.
34. Jadhav, A.P.; Mason, H.A.; Cepko, C.L. Notch 1 inhibits photoreceptor production in the developing mammalian retina. *Development* **2006**, *133*, 913–923.
35. Ohata, S.; Aoki, R.; Kinoshita, S.; Yamaguchi, M.; Tsuruoka-Kinoshita, S.; Tanaka, H.; Wada, H.; Watabe, S.; Tsuboi, T.; Masai, I.; et al. Dual Roles of Notch in Regulation of Apically Restricted Mitosis and Apicobasal Polarity of Neuroepithelial Cells. *Neuron* **2011**, *69*, 215–230.
36. Herranz, H.; Stamataki, E.; Feiguin, F.; Milán, M. Self-refinement of notch activity through the transmembrane protein crumbs: Modulation of γ-secretase activity. *EMBO Rep.* **2006**, *7*, 297–302.
37. Nemetschke, L.; Knust, E. Drosophila Crumbs prevents ectopic Notch activation in developing wings by inhibiting ligand-independent endocytosis. *Development* **2016**, *143*, 4543–4553.
38. Ridley, S.H.; Ktistakis, N.; Davidson, K.; Anderson, K.E.; Manifava, M.; Ellson, C.D.; Lipp, P.; Bootman, M.; Coadwell, J.; Nazarian, A.; et al. FENS-1 and DFCP1 are FYVE domain-containing proteins with distinct functions in the endosomal and Golgi compartments. *J. Cell Sci.* **2001**, *114*, 3991–4000.
39. Gajović, S.; Mitrečić, D.; Augustinčić, L.; Iaconcig, A.; Muro, A.F. Unexpected rescue of alpha-synuclein and multimerin1 deletion in C57BL/6JOlaHsd mice by beta-adducin knockout. *Transgenic Res.* **2006**, *15*, 255–259.
40. Ha, T.; Moon, K.H.; Dai, L.; Hatakeyama, J.; Yoon, K.; Park, H.-S.; Kong, Y.-Y.; Shimamura, K.; Kim, J.W. The Retinal Pigment Epithelium Is a Notch Signaling Niche in the Mouse Retina. *Cell Rep.* **2017**, *19*, 351–363.
41. Yaron, O.; Farhy, C.; Marquardt, T.; Applebury, M.; Ashery-Padan, R. Notch1 functions to suppress cone-photoreceptor fate specification in the developing mouse retina. *Development* **2006**, *133*, 1367–1378.
42. Richardson, E.C.N.; Pichaud, F. Crumbs is required to achieve proper organ size control during Drosophila head development. *Development* **2010**, *137*, 641–650.
43. Rosa-Ferreira, C.; Munro, S. Arl8 and SKIP Act Together to Link Lysosomes to Kinesin-1. *Dev. Cell* **2011**, *21*, 1171–1178.
44. Farfel-Becker, T.; Roney, J.C.; Cheng, X.T.; Li, S.; Cuddy, S.R.; Sheng, Z.H. Neuronal Soma-Derived Degradative Lysosomes Are Continuously Delivered to Distal Axons to Maintain Local Degradation Capacity. *Cell Rep.* **2019**, *28*, 51-64.e4.
45. Overhoff, M.; De Bruyckere, E.; Kononenko, N.L. Mechanisms of neuronal survival safeguarded by endocytosis and autophagy. *J. Neurochem.* **2021**, *157*, 263–296.
46. Pradhan, J.; Noakes, P.G.; Bellingham, M.C. The Role of Altered BDNF/TrkB Signaling in Amyotrophic Lateral Sclerosis. *Front. Cell. Neurosci.* 2019, *13*, 368.
47. Babu, J.R.; Seibenhener, M.L.; Peng, J.; Strom, A.-L.; Kemppainen, R.; Cox, N.; Zhu, H.; Wooten, M.C.; Diaz-Meco, M.T.; Moscat, J.; et al. Genetic inactivation of p62 leads to accumulation of hyperphosphorylated tau and neurodegeneration. *J. Neurochem.* **2008**, *106*, 107–120.
48. Kakar-Bhanot, R.; Brahmbhatt, K.; Chauhan, B.; Katkam, R.R.; Bashir, T.; Gawde, H.; Mayadeo, N.; Chaudhari, U.K.; Sachdeva, G. Rab11a drives adhesion molecules to the surface of endometrial epithelial cells. *Hum. Reprod.* **2019**, *34*.
49. Aguilar-Aragon, M.; Fletcher, G.; Thompson, B.J. The cytoskeletal motor proteins Dynein and MyoV direct apical transport of Crumbs. *Dev. Biol.* **2020**, *459*, 126–137.
50. Gaullier, J.-M.; Simonsen, A.; D'Arrigo, A.; Bremnes, B.; Stenmark, H.; Aasland, R. FYVE fingers bind PtdIns(3)P. *Nat. 1998 3946692* **1998**, *394*, 432–433.
51. Bellingrath, J.-S.; McClements, M.E.; Kaukonen, M.; Fischer, M.D.; MacLaren, R.E. In Silico Analysis of Pathogenic CRB1 Single Nucleotide Variants and Their Amenability to Base Editing as a Potential Lead for Therapeutic Intervention. *Genes 2021, Vol. 12, Page 1908* **2021**, *12*, 1908.
52. Trousdale, C.; Kim, K. Retromer: Structure, function, and roles in mammalian disease. *Eur. J. Cell Biol.* **2015**, *94*, 513–521.

53. Wang, S.; Tan, K.L.; Agosto, M.A.; Xiong, B.; Yamamoto, S.; Sandoval, H.; Jaiswal, M.; Bayat, V.; Zhang, K.; Charng, W.-L.; et al. The Retromer Complex Is Required for Rhodopsin Recycling and Its Loss Leads to Photoreceptor Degeneration. *PLoS Biol.* **2014**, *12*, 1001847.
54. Boon, N.; Wijnholds, J.; Pellissier, L.P. Research Models and Gene Augmentation Therapy for CRB1 Retinal Dystrophies. *Front. Neurosci.* **2020**, *14*, 860.
55. Clark, B.S.; Miesfeld, J.B.; Flinn, M.A.; Collery, R.F.; Link, B.A. Dynamic Polarization of Rab11a Modulates Crb2a Localization and Impacts Signaling to Regulate Retinal Neurogenesis. *Front. Cell Dev. Biol.* **2021**, *8*, 608112.
56. Campa, C.C.; Margaria, J.P.; Derle, A.; Del Giudice, M.; De Santis, M.C.; Gozzelino, L.; Copperi, F.; Bosia, C.; Hirsch, E. Rab11 activity and PtdIns(3)P turnover removes recycling cargo from endosomes. *Nat. Chem. Biol. 2018 148* **2018**, *14*, 801–810.
57. Pellissier, L.P.; Quinn, P.M.; Henrique Alves, C.; Vos, R.M.; Klooster, J.; Flannery, J.G.; Alexander Heimel, J.; Wijnholds, J. Gene therapy into photoreceptors and Müller glial cells restores retinal structure and function in CRB1 retinitis pigmentosa mouse models. *Hum. Mol. Genet.* **2015**, *24*, 3104–3118.
58. Alves, C.H.; Sanz, A.S.; Park, B.; Pellissier, L.P.; Tanimoto, N.; Beck, S.C.; Huber, G.; Murtaza, M.; Richard, F.; Sridevi Gurubaran, I.; et al. Loss of CRB2 in the mouse retina mimics human retinitis pigmentosa due to mutations in the CRB1 gene. *Hum. Mol. Genet.* **2013**, *22*, 35–50.
59. Rowan, S.; Cepko, C.L. Genetic analysis of the homeodomain transcription factor Chx10 in the retina using a novel multifunctional BAC transgenic mouse reporter. *Dev. Biol.* **2004**, *271*, 388–402.
60. Kolisnyk, B.; Guzman, M.S.; Raulic, S.; Fan, J.; Magalhães, A.C.; Feng, G.; Gros, R.; Prado, V.F.; Prado, M.A.M. Chat-ChR2-EYFP mice have enhanced motor endurance but show deficits in attention and several additional cognitive domains. *J. Neurosci.* **2013**, *33*, 10427–10438.
61. Ting, J.T.; Feng, G. Recombineering strategies for developing next generation BAC transgenic tools for optogenetics and beyond. *Front. Behav. Neurosci.* **2014**, *8*, 1–13.
62. Specht, C.G.; Schoepfer, R. Deletion of multimerin-1 in α-synuclein-deficient mice. *Genomics* **2004**, *83*, 1176–1178.
63. Huang, T.T.; Naeemuddin, M.; Elchuri, S.; Yamaguchi, M.; Kozy, H.M.; Carlson, E.J.; Epstein, C.J. Genetic modifiers of the phenotype of mice deficient in mitochondrial superoxide dismutase. *Hum. Mol. Genet.* **2006**, *15*, 1187–1194.
64. Alves, C.H.; Wijnholds, J. AAV gene augmentation therapy for CRB1-associated retinitis pigmentosa. In *Methods in Molecular Biology*; Boon, C.J.F., Wijnholds, J., Eds.; Humana Press Inc.: New York, NY, 2018; Vol. 1715, pp. 135–151 ISBN 9781493975211.
65. Robinson, M.D.; McCarthy, D.J.; Smyth, G.K. edgeR: a Bioconductor package for differential expression analysis of digital gene expression data. *Bioinformatics* **2010**, *26*, 139–140.
66. Ritchie, M.E.; Phipson, B.; Wu, D.; Hu, Y.; Law, C.W.; Shi, W.; Smyth, G.K. limma powers differential expression analyses for RNA-sequencing and microarray studies. *Nucleic Acids Res.* **2015**, *43*, e47–e47.
67. Robinson, M.D.; Oshlack, A. A scaling normalization method for differential expression analysis of RNA-seq data. *Genome Biol.* **2010**, *11*.
68. Law, C.W.; Chen, Y.; Shi, W.; Smyth, G.K. voom: Precision weights unlock linear model analysis tools for RNA-seq read counts. *Genome Biol.* **2014**, *15*.
69. Faas, F.G.A.; Cristina Avramut, M.; van den Berg, B.M.; Mieke Mommaas, A.; Koster, A.J.; Ravelli, R.B.G. Virtual nanoscopy: Generation of ultra-large high resolution electron microscopy maps. *J. Cell Biol.* **2012**, *198*, 457–469.

Figures

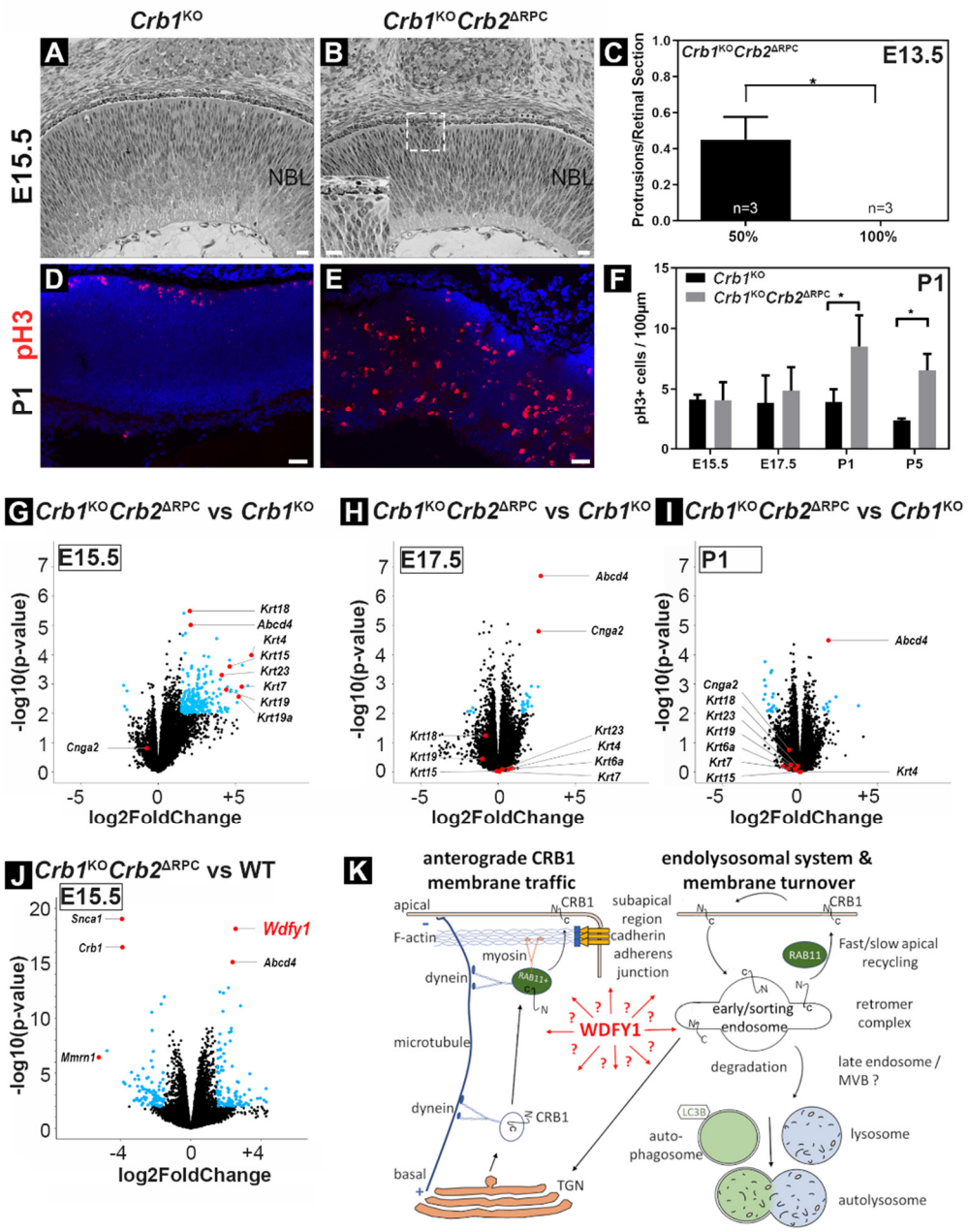
Crb1KO
Crb1KOCrb2ΔRPC
A
B
C
E15.5
NBL
NBL
Crb1KOCrb2ΔRPC E13.5
Protrusions/Retinal Section
n=3
n=3
50%
100%
D
E
F
P1
pH3
Crb1KO
Crb1KOCrb2ΔRPC
P1
pH3+ cells / 100µm
E15.5
E17.5
P1
P5
G Crb1KOCrb2ΔRPC vs Crb1KO
H Crb1KOCrb2ΔRPC vs Crb1KO
I Crb1KOCrb2ΔRPC vs Crb1KO
E15.5
E17.5
P1
-log10(p-value)
log2FoldChange
Krt18
Abcd4
Krt4
Krt15
Krt23
Krt7
Krt19
Krt19a
Cnga2
Krt6a
J Crb1KOCrb2ΔRPC vs WT
E15.5
Snca1
Crb1
Mmrn1
Wdfy1
Abcd4
K
anterograde CRB1 membrane traffic
endolysosomal system & membrane turnover
apical
CRB1
F-actin
myosin
dynein
RAB11a
microtubule
basal
TGN
subapical region cadherin adherens junction
WDFY1
RAB11
Fast/slow apical recycling
retromer complex
early/sorting endosome
degradation
late endosome / MVB ?
LC3B
auto-phagosome
lysosome
autolysosome

Figure 1. **mRNA transcript levels are marginally different in *Crb1*^{KO}*Crb2*$^{\Delta RPC}$ against *Crb1*^{KO} neuroretina.** (A-B) Retinal morphology on plastic sections of *Crb1*^{KO} and *Crb1*^{KO}*Crb2*$^{\Delta RPC}$ mice on 100% C57/B6 genetic background at E15.5. (A) *Crb1*^{KO} retinas appeared unaffected while (B) *Crb1*^{KO}*Crb2*$^{\Delta RPC}$ retinas had protrusions of NBL nuclei in the subretinal space (insert). (C) Protrusions per retinal section in 50% and 100% C57/B6 genetic background at E13.5. (D-J) 100% C57/B6 genetic background. (D-E) Immunofluorescence labelling of pH3+ nuclei (late G2 cell cycle and mitosis maker) at P1 in (D) *Crb1*^{KO} and (E) and *Crb1*^{KO}*Crb2*$^{\Delta RPC}$ retina. (F) Quantification of pH3+ cells at E15.5, E17.5, P1, and P5. (G-J) All changed genes indicated in blue circles (p -value < 0.01; log2fc > 1.5). (G-I) *Crb1*^{KO}*Crb2*$^{\Delta RPC}$ against *Crb1*^{KO} neuroretina transcripts (Run1) at embryonic day (E)15.5, E17.5, and P1. (J) *Crb1*^{KO}*Crb2*$^{\Delta RPC}$ compared to WT neuroretina transcripts at E15.5 (Run2). (K) Potential WDFY1 involvement in CRB1 protein trafficking (modified from [49]). Scale bar, 20 µm. WT, wildtype; TGN, trans golgi network; MVB, multivesicular body. See also Figure S1+S2.

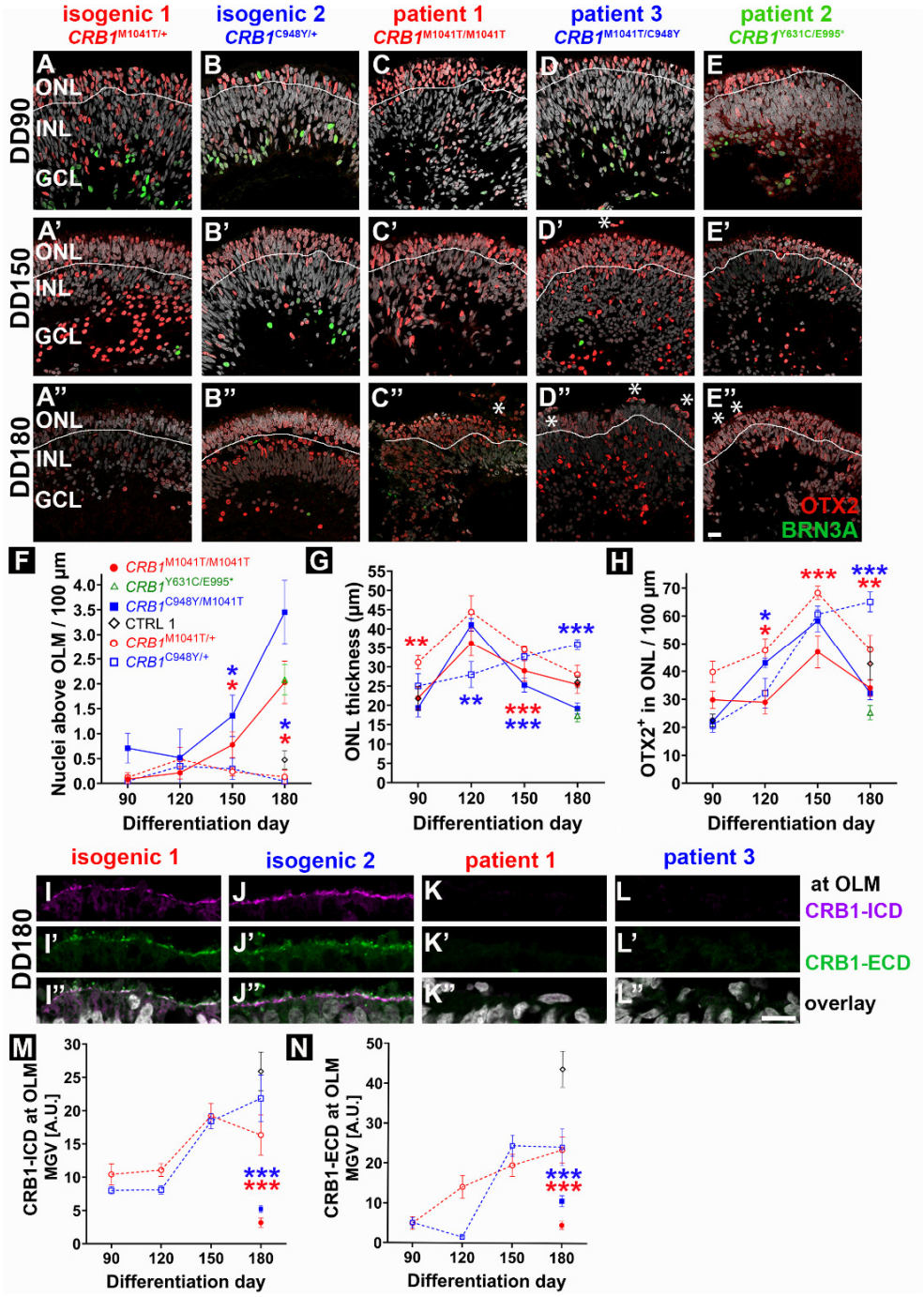
isogenic 1
CRB1M1041T/+
isogenic 2
CRB1C948Y/+
patient 1
CRB1M1041T/M1041T
patient 3
CRB1M1041T/C948Y
patient 2
CRB1Y631C/E995*
DD90
DD150
DD180
ONL
INL
GCL
OTX2
BRN3A
Nuclei above OLM / 100 µm
ONL thickness (µm)
OTX2+ in ONL / 100 µm
Differentiation day
CTRL 1
at OLM
CRB1-ICD
CRB1-ECD
overlay
CRB1-ICD at OLM MGV [A.U.]
CRB1-ECD at OLM MGV [A.U.]

Figure 2. CRB1 patient organoids degenerate over time and express little CRB1 apically. (A-E) Nuclei stained for OTX2 (early photoreceptor cells) and BRN3A (Ganglion cells; scale bar, 50 µm). (A-B) isogenic control, (C-E) CRB1 patient organoids at DD90 (A-E), DD150 (A'-E'), DD180 (A''-E''). Ectopic nuclei are indicated with an asterisk and ONL/INL border with a white line. (F) number of nuclei above the OLM over time, (G) number of ONL thickness over time (OTX2+/DAPI+ nuclei top layer), (H)) OTX2+ photoreceptor loss over time (F-H: n=9-25). (I-L) CRB1 stained with an (I-L) intracellular (ICD) or (I'-L') extracellular domain (ECD) epitope antibodies at the OLM, and (I''-L'') overlay (scale bar, 10 µm). (M-N) CRB1-Alexa conjugated fluorescence signal detected over time on ICD-(M) and ECD-(N) CRB1 antibodies (empty circles/dashed lines, isogenic controls; filled circles, patient lines; DD180, n=8; DD90-150, n=4-6 organoids per line). isogenic 1: CRB1Met1041Thr/ +, iso03LUMC0116iCRB09; isogenic 2: CRB1Cys948Tyr/+, iso02LUMC0128iCRB01; Patient 1 to 3: CRB1Met1041Thr/ Met1041Thr, LUMC0116iCRB09; CRB1Tyr631Cys/Glu995*, LUMC0117iCRB01; CRB1Met1041Thr/Cys948Tyr, LUMC0128iCRB01. OLM, outer nuclear layer; MVG, mean gray value. See also Figure S3+S4.

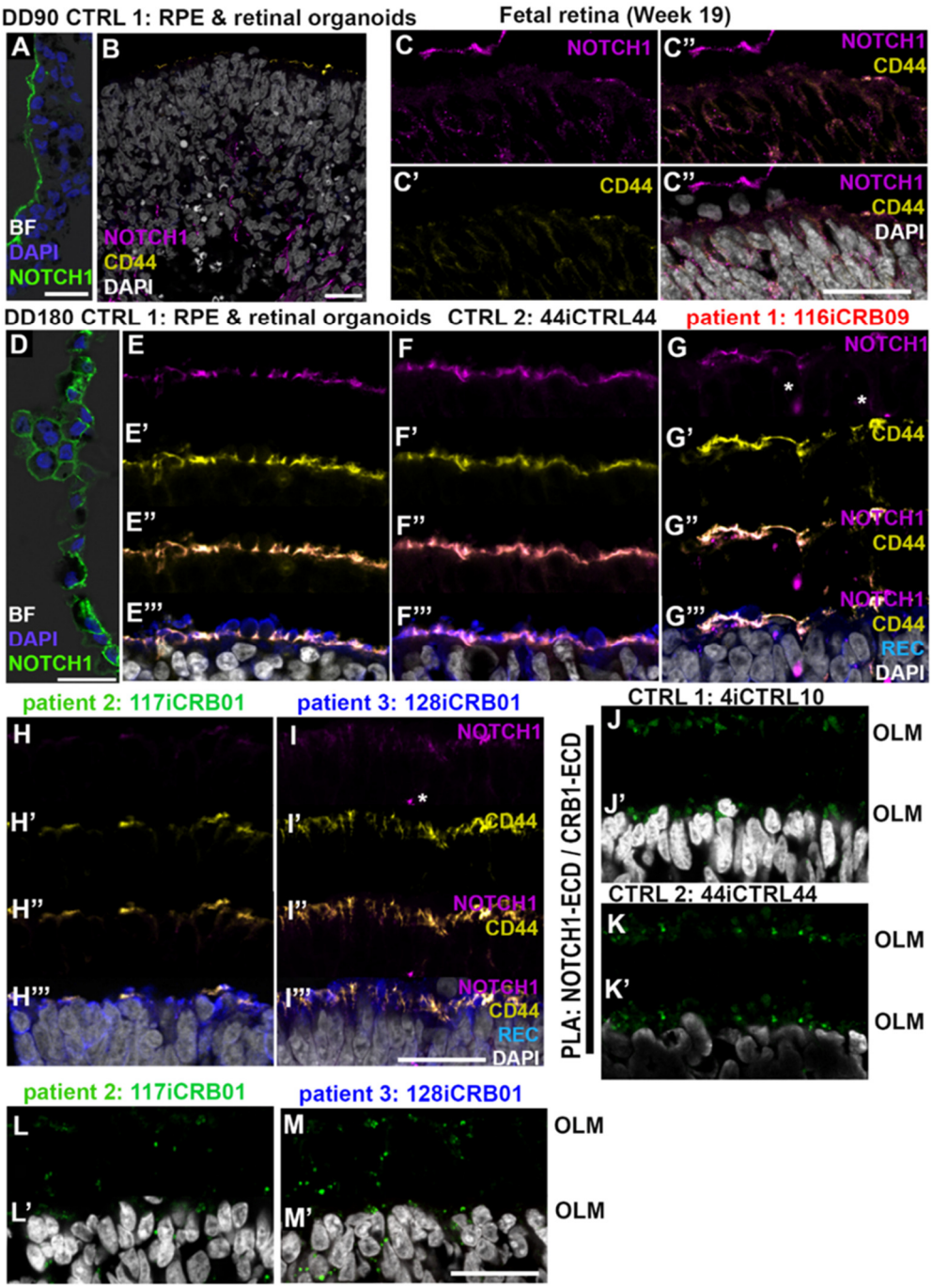
DD90 CTRL 1: RPE & retinal organoids
Fetal retina (Week 19)
A
B
C
C'
C''
BF
DAPI
NOTCH1
CD44
DD180 CTRL 1: RPE & retinal organoids
CTRL 2: 44iCTRL44
patient 1: 116iCRB09
D
E
E'
E''
E'''
F
F'
F''
F'''
G
G'
G''
G'''
REC
patient 2: 117iCRB01
patient 3: 128iCRB01
H
H'
H''
H'''
I
I'
I''
I'''
CTRL 1: 4iCTRL10
CTRL 2: 44iCTRL44
PLA: NOTCH1-ECD / CRB1-ECD
J
J'
K
K'
OLM
L
L'
M
M'

Figure 3. Apical NOTCH1 is lost in *CRB1* patient retinal organoids. (A+D) CTRL1 (LUMC004iCTRL10) RPE expresses NOTCH1 at DD90 and DD180. (B) Little NOTCH1 is expressed at the OLM in the CTRL1 DD90 retinal organoid. (C) NOTCH1 is expressed in the RPE and very little in the neuroretina at the OLM in human fetal retina (gestation week 19). (E) CTRL1, (F) CTRL2 (LUMC044iCTRL44), (G) patient 1 (LUMC0116iCRB09), (H) patient 2 (LUMC0117iCRB01), patient 3 (LUMC0128iCRB01). (E-I) NOTCH1 is expressed specifically in DD180 Müller glial apical villi (magenta, NOTCH1; yellow, CD44; blue, recoverin; gray, DAPI). (J-M) Proximity Ligation Assay of NOTCH1-ECD and CRB1-ECD (green signal) shows interaction at control OLM, but reduced interaction at patient OLM with increased localization in patient ONL. Scale bar, 25 µm.

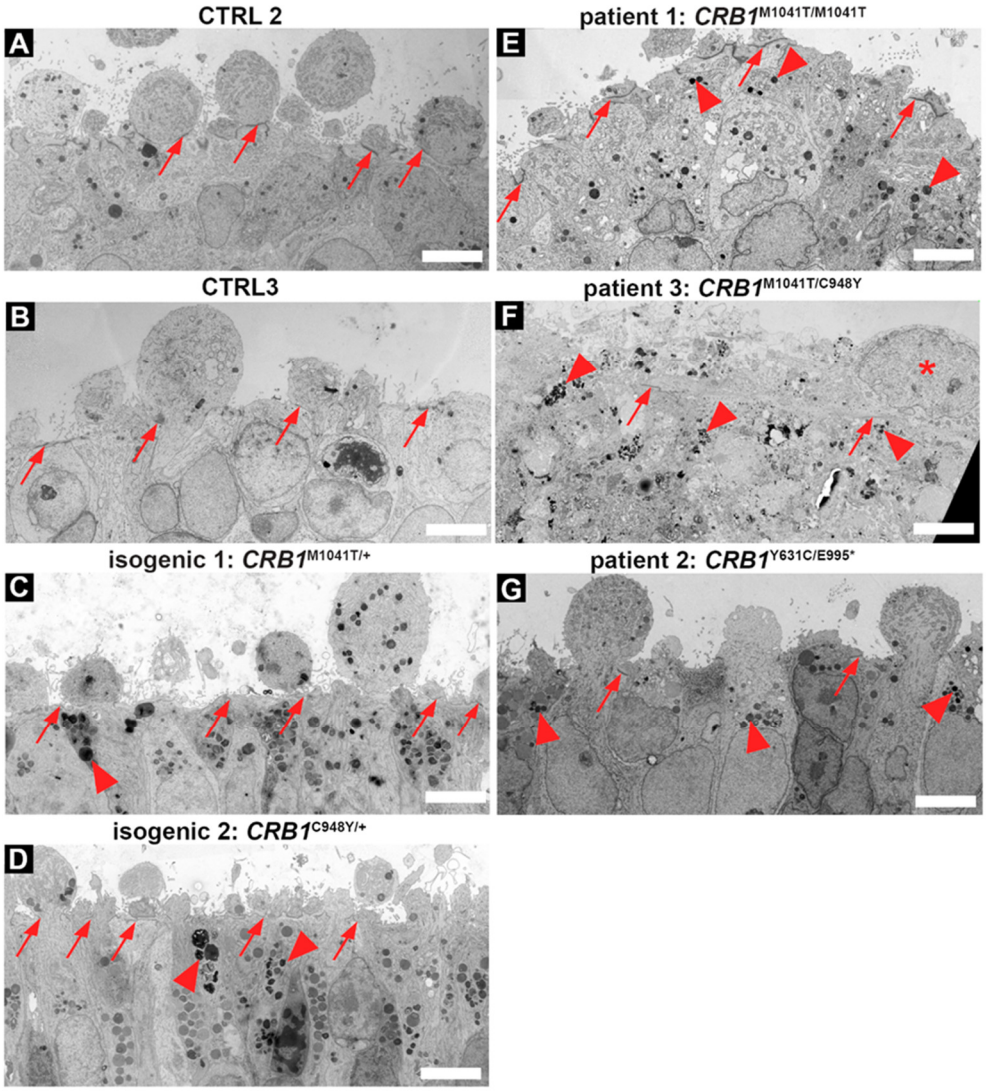

Figure 4. Transmission electron microscopy high resolution imaging of retinal organoids at DD180. Electron-dense outer limiting membrane (red arrows), electron-dense degradative compartments/vacuoles (arrowheads), and nuclei above OLM (asterisks). (A-B) control lines (LUMC0044iCTRL44; LUMC080iCTRL12), (C-D) gene corrected lines (iso3LUMC0116iCRB09; iso2LUMC0128iCRB01), and (E-G) patient lines (LUMC0116iCRB09; LUMC0117iCRB01; LUMC0128iCRB01). Scale bar, 5 µm.

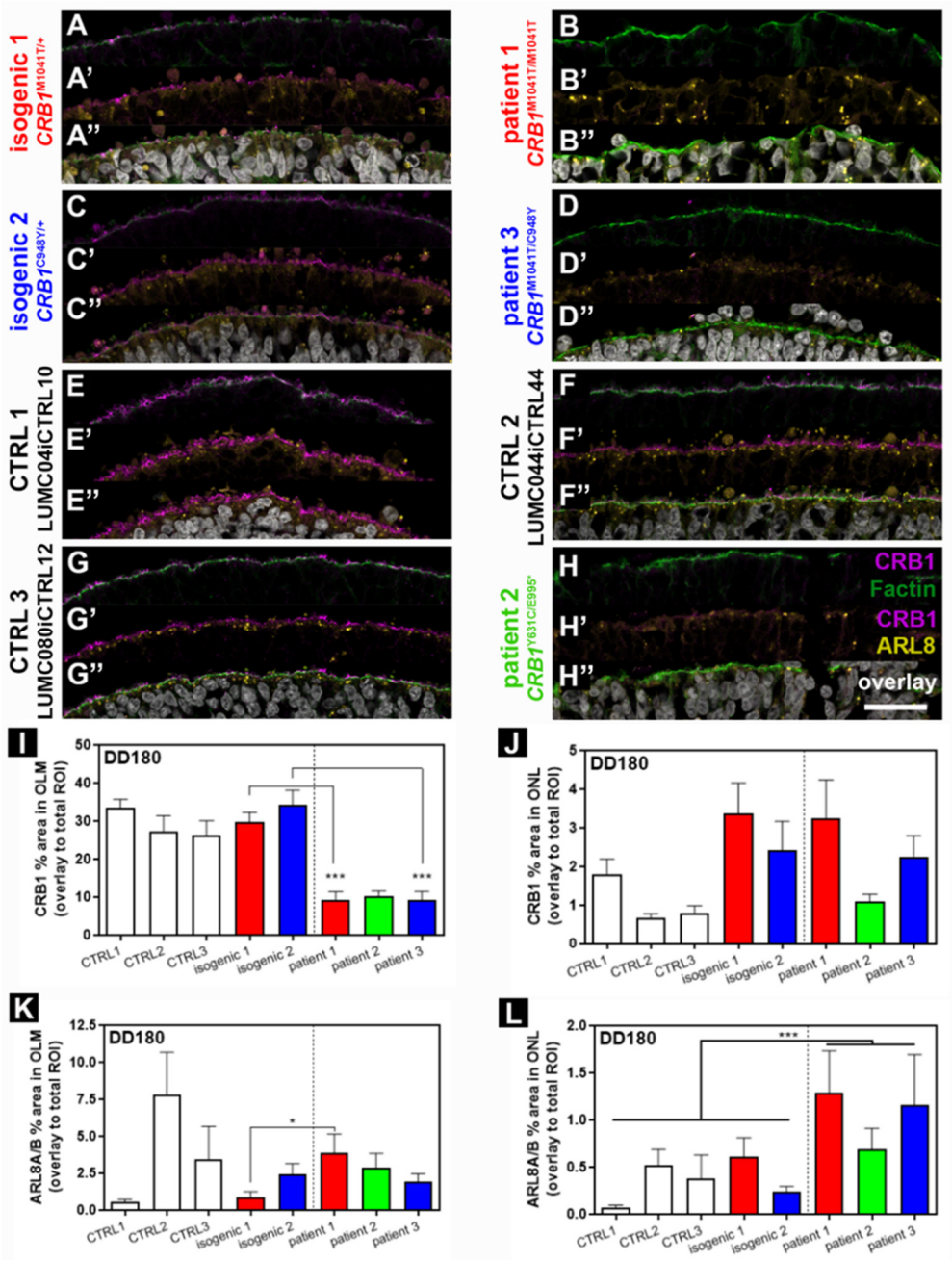

Figure 5. Immunofluorescence signal of CRB1 labelling is reduced in *CRB1* patient retinal organoids at the OLM. (A-H) Triple staining of CRB1 (magenta), phalloidin (filamentous actin, F-actin; green), and ARL8A/B (yellow). (I-J) CRB1-fluorescence signal measured by puncta in the OLM and ONL. (K-L) CRB1-fluorescence signal measured by puncta in the OLM and ONL. N=6-14 organoids per line. Scale bar, 25 µm.

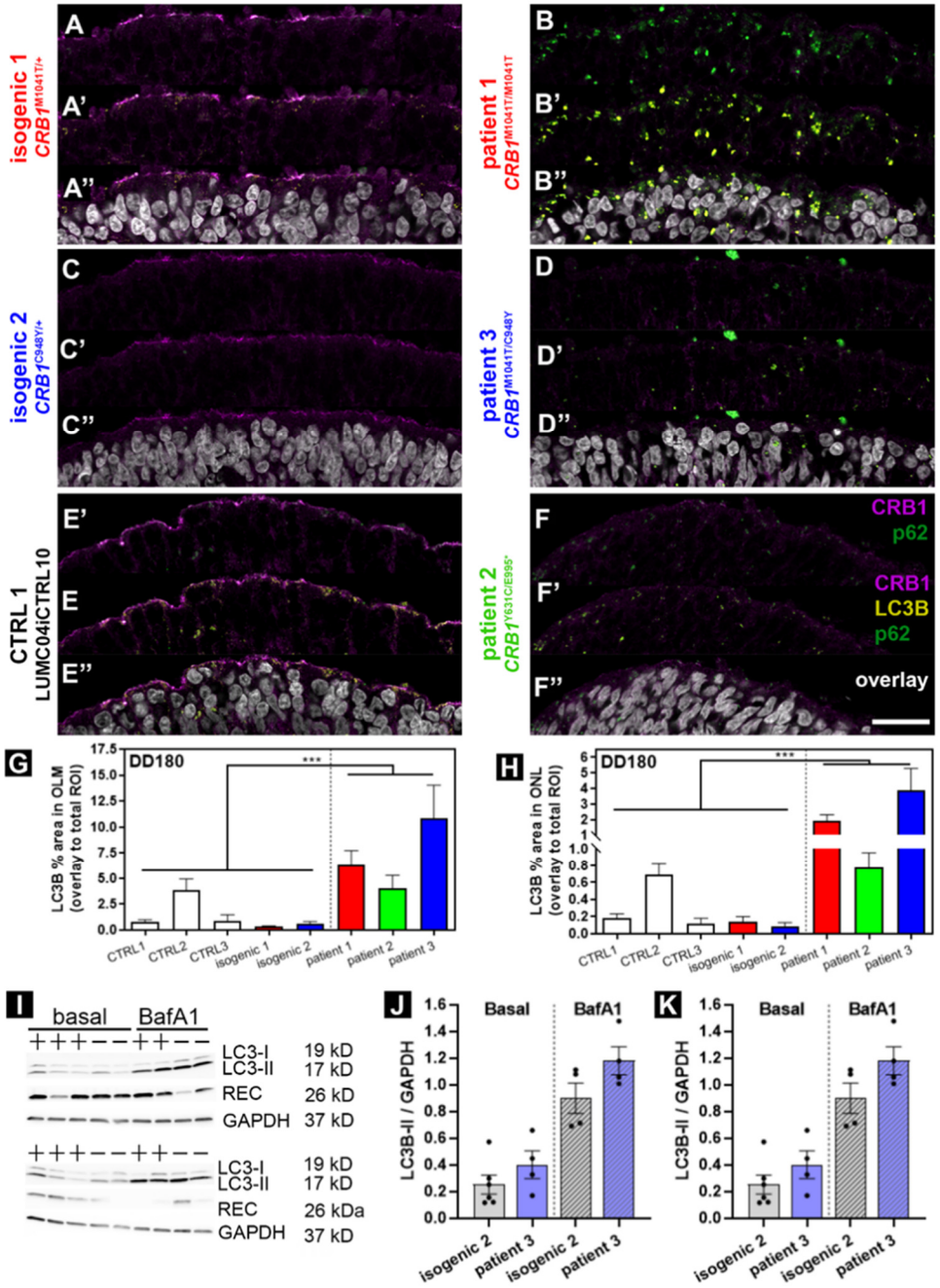

Figure 6. More degradative vesicles/compartments are present in *CRB1* patient retinal organoids. (A-F) Immunofluorescence triple staining CRB1 (magenta), p62 (green), and LC3B (yellow). (G-H) LC3B localized more in the ONL and OLM layers in *CRB1* RP retinal organoids. (I-K) Western blot of individual lysed organoids (plus symbol, isogenic 2 line (iso02-128iCRB01)); minus symbol, patient 3 (line LUMC0128CRB01) stained for LC3B (LC3-I and LC3-II; 19/17 kD; recoverin for photoreceptors (26 kD), and GAPDH (housekeeping control, 37 kD). The autophagic flux was decreased in *CRB1* patient organoids. Scale bar, 25 µm.

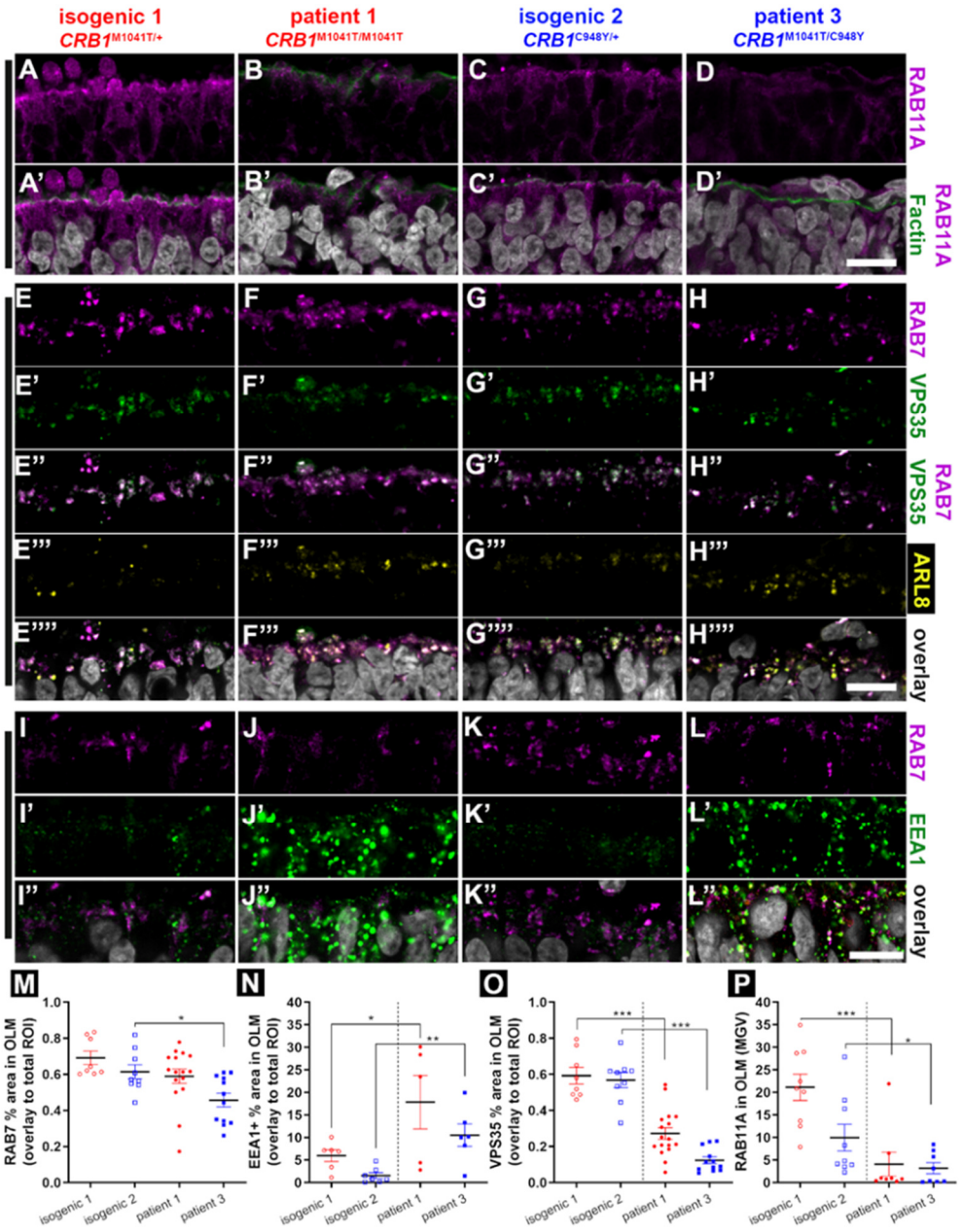

Figure 7. Dysregulation of the endolysosomal system in *CRB1* patient organoids. Immunofluorescence on isogenic control lines 1 and 2 (A+C; E+G; I+K) related to the patient lines 1 (LUMC0116iCRB09) and patient line 3 (LUMC0128iCRB01), and patient lines 1+3 (B+D; F+H; J-L). (A-D) recycling endosomes (RAB11A; magenta) and phalloidin (F-actin; green). (E-H) late endosomes (RAB7; magenta), retromer complex (VPS35; green), endolysosomes (ARL8A/B; yellow). (I-L) late endosomes (RAB7, mangenta) and early endosomes (EEA1, green) and. (M-P) Quantification of fluorescence signal of early endosomes (EEA1), late endosomes (RAB7), retromer (VSP35), and recycling endosomes (RAB11A) in OLM. (M) RAB7 in OLM. (N) EEA1 in OLM. (O) VPS35 in OLM. (P) RAB11A in OLM. Scale bar, 10 µm.

Supplemental Information

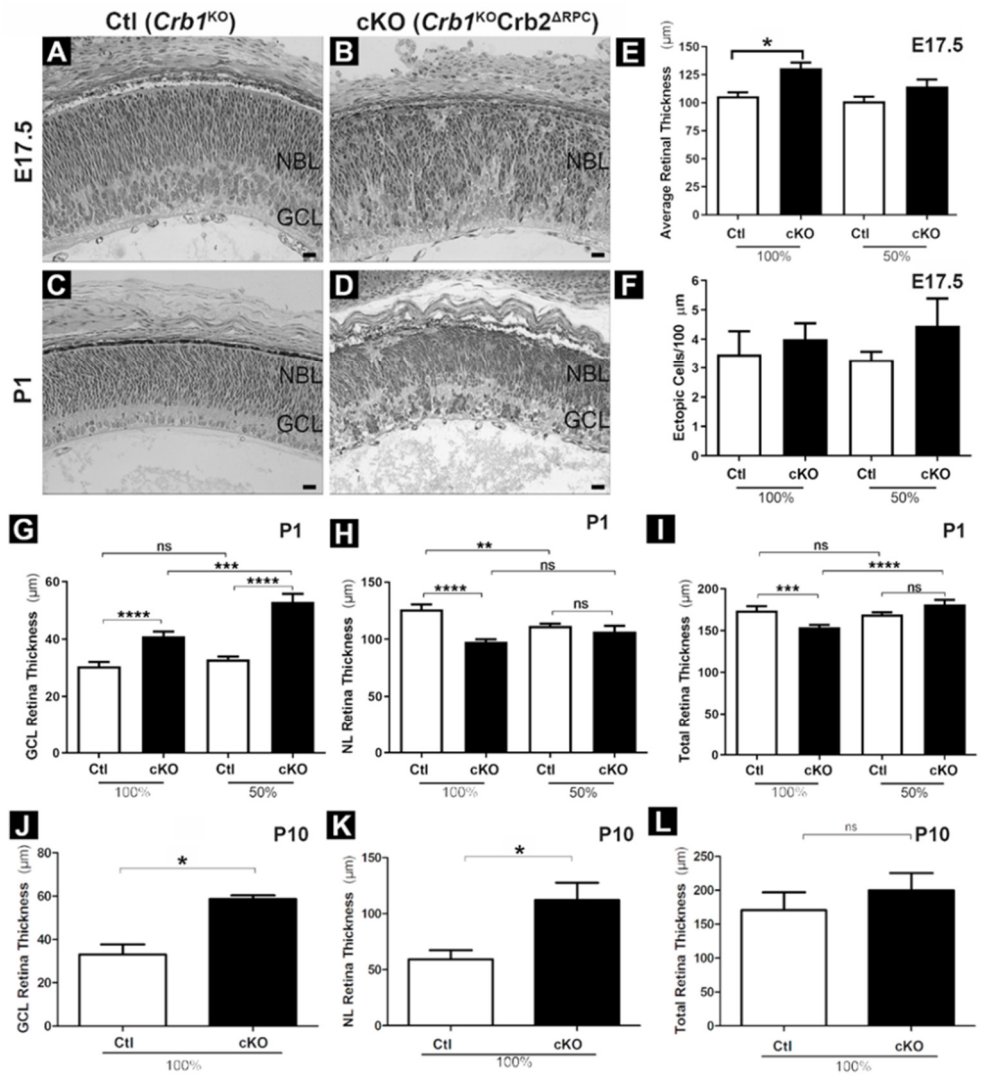

Figure S1. The retinal morphological phenotype is milder in *Crb1*^{KO}*Crb2*$^{\Delta RPC}$ on 100% C57/B6 genetic background than on 50% mixed genetic background. Related to Figure 1. (A-D) Retinal morphology on plastic sections of Ctl (*Crb1*^{KO}) and cKO (*Crb1*^{KO}*Crb2*$^{\Delta RPC}$) mice on 100% C57/B6 genetic background at E17.5 and P1. (E-F) Ctl (*Crb1*^{KO}) and cKO (*Crb1*^{KO}*Crb2*$^{\Delta RPC}$) mice on 50% and 100% C57/B6 genetic background. (E-F) Average retinal thickness and ectopic nuclei per 100 µm retinal length at E17.5. (G-I) Ganglion cell layer (GCL) thickness, neuroretina layer (NL) thickness, and retinal thickness (OLM-ILM) at P1. (J-L) GCL thickness, NL thickness, and retinal thickness in 100% C57/B6 genetic background at P10. Scale bar, 20 µm.

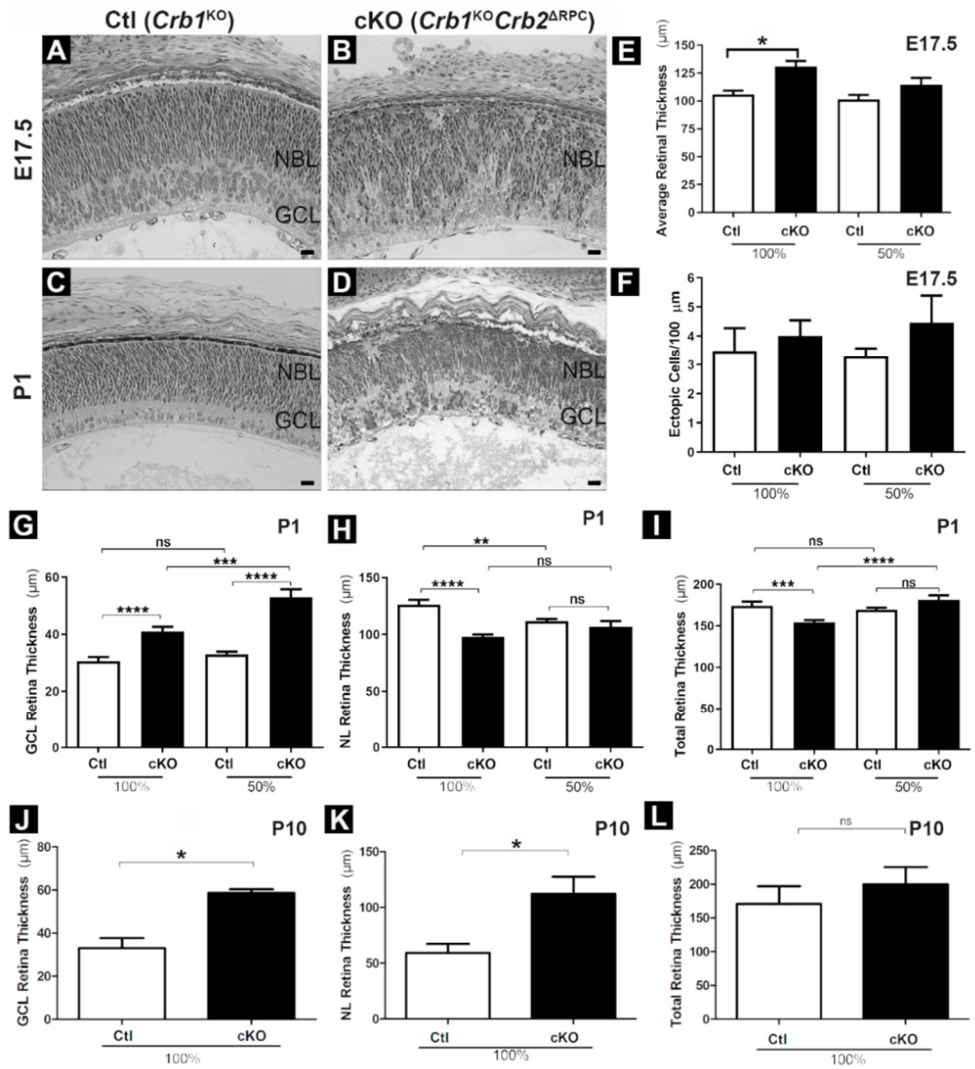

Figure S2. The *Crb1*^{KO}*Crb2*$^{\Delta RPC}$ mouse displays an LCA-like *CRB1* phenotype. Related to Figure 1. (A-F) Retinal morphology on plastic sections of Ctl (*Crb1*^{KO}) and cKO (*Crb1*^{KO}*Crb2*$^{\Delta RPC}$) mice on 100% C57/B6 genetic background at P14, 1M, and 3M. (G-H) Retinal thickness (OLM-ILM) at P14, 1M, and 3M. (I-K) Electroretinographic (ERG) analysis of the retinal function at 1M. Conditional KOs are in red and Ctl age-matched littermates in gray: (L-M) Scotopic (SC) single-flash intensity series (-4, -3 , -2, -1, 0, 1, 1.5, 1.9 log cd s/m² light intensity). (I) scotopic a-wave amplitudes. (J) scotopic b-wave amplitudes. (K) Photopic (PH) single-flash ERG at different light intensities (-2, -1, 0, 1, 1.5, 1.9 log cd s/m² light intensity at 30 cd/m² background light). Boxes indicate the 25 and 75% quantile range, whiskers indicate the 5 and 95% quantiles, and the intersection of line and error bar indicates the median of the data. (L) *Crb1*^{KO}*Crb2*$^{\Delta RPC}$ vs *Crb1*^{KO} neuroretina qPCR validation (n=5 retinas / group) of transcript changes at P1. Statistical significance calculated by a two-sided T-Test ($p<0.05$; 0.01; 0.001 shown as *, **, and ***). Scale bar, 20 µm.

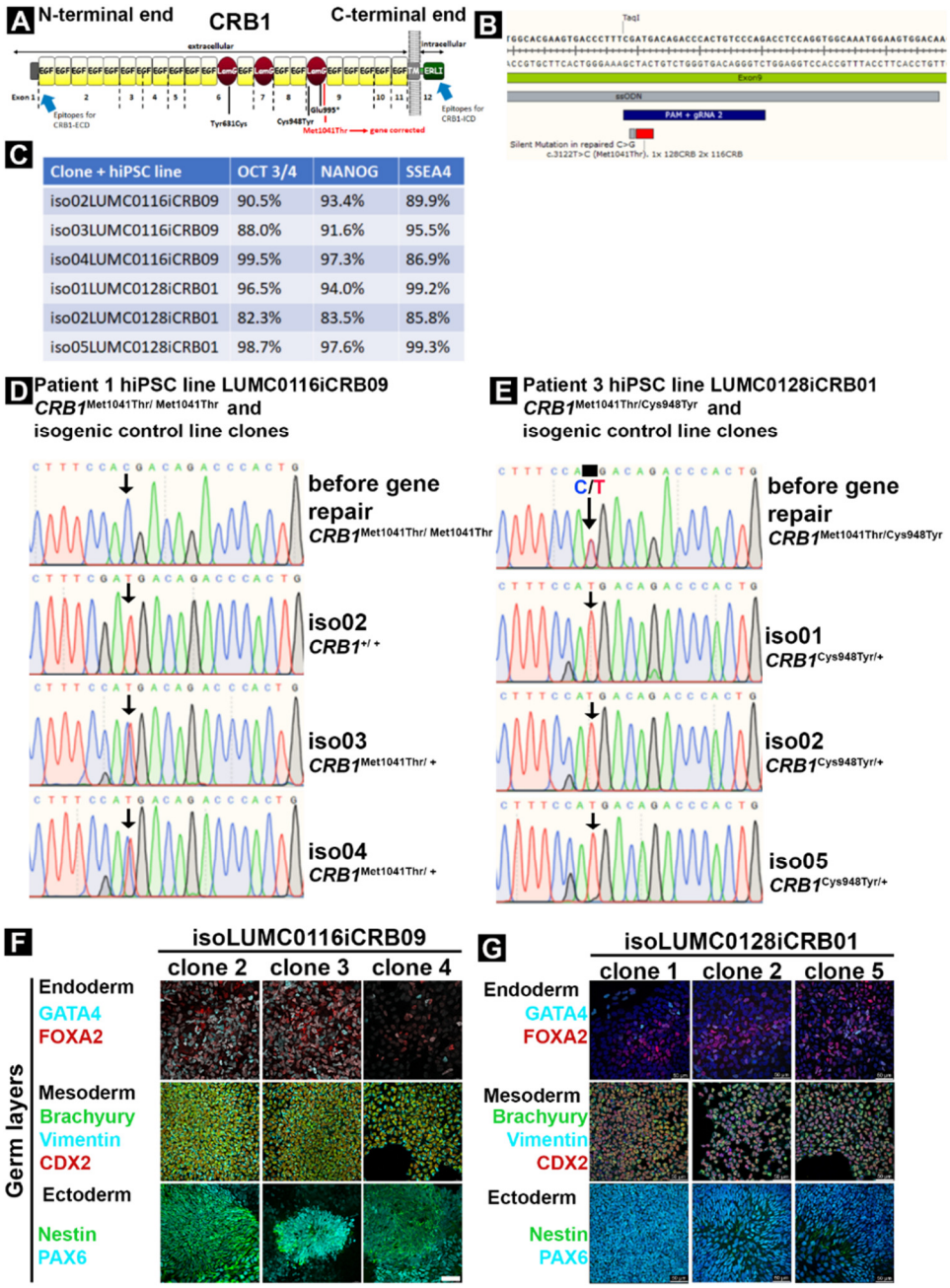

Figure S3. Validation of the isogenic control iPS cell lines. Related to Figure 2-7. (A) CRB1 protein domains and the corresponding exons, CRB1 patient variants, and the epitope of the CRB1-ICD and CRB-ECD antibodies. (B) Gene correction by single-stranded oligodeoxynucleotides (ssODN), gRNA, and nuclease Cas9 on locus c.3122T>C. (C) Flow cytometry sorted human iPSC clones indicating expression of pluripotency markers SSEA4, OCT3/4, and NANOG. (D-E) Sanger sequence validation of 3 clones per patient line. (G-H) human iPSC clones differentiated into the three germ layers. Scale bar, 50 µm.

Clone + hiPSC line	OCT 3/4	NANOG	SSEA4
iso02LUMC0116iCRB09	90.5%	93.4%	89.9%
iso03LUMC0116iCRB09	88.0%	91.6%	95.5%
iso04LUMC0116iCRB09	99.5%	97.3%	86.9%
iso01LUMC0128iCRB01	96.5%	94.0%	99.2%
iso02LUMC0128iCRB01	82.3%	83.5%	85.8%
iso05LUMC0128iCRB01	98.7%	97.6%	99.3%

Table S1. Information on human iPSC lines. Related to Figure S3 and Figure 2-7.

Line code	Description	Gender
Control-derived and gene corrected (isogenic, iso) human iPSC line names		
LUMC0004iCTRL10	Control line 1 (CTRL 1)	male
LUMC0044iCTRL44	Control line 2 (CTRL 2)	female
LUMC0080iCTRL12	Control line 3 (CTRL 3)	male
iso01LUMC0116iCRB09	isogenic: Allele 1: c.3122T>C gene corrected to c.3122C>T. Allele 2: c.3122T>C. p.(Met1041Thr)	male
iso02LUMC0116iCRB09	isogenic 1: Allele 1: c.3122T>C gene corrected to c.3122C>T. Allele 2: c.3122T>C. p.(Met1041Thr)	male
iso03LUMC0116iCRB09	isogenic: Allele 1 and 2: Homozygous c.3122T>C gene corrected to c.3122C>T	male
iso01LUMC0128iCRB01	isogenic: Allele 1: c.2843G>A --> p.(Cys948Tyr). Allele 2: c.3122T>C gene corrected to c.3122C>T	male
iso02LUMC0128iCRB01	Isogenic 2: Allele 1: c.2843G>A. p.(Cys948Tyr). Allele 2: c.3122T>C gene corrected to c.3122C>T	male
iso03LUMC0128iCRB01	isogenic: Allele 1: c.2843G>A. p.(Cys948Tyr). Allele 2: c.3122T>C gene corrected to c.3122C>T	male
iso05LUMC0128iCRB01	isogenic: Allele 1: c.2843G>A. p.(Cys948Tyr). Allele 2: c.3122T>C gene corrected to c.3122C>T	male
Patient *CRB1* Retinitis pigmentosa-derived human iPSC lines		
LUMC0116iCRB09	Patient 1. Allele 1 and 2: homozygous c.3122T>C--> p.(Met1041Thr)	male
LUMC0117iCRB01	Patient 2. Allele 1: c.1892A>G (p.Tyr631Cys)). Allele 2: c.2911G>T (p.(Glu995*))	male
LUMC0128iCRB01	Patient 3. Allele 1: c.2843G>A --> p.(Cys948Tyr). Allele 2: c.3122T>C --> p.(Met1041Thr)	male

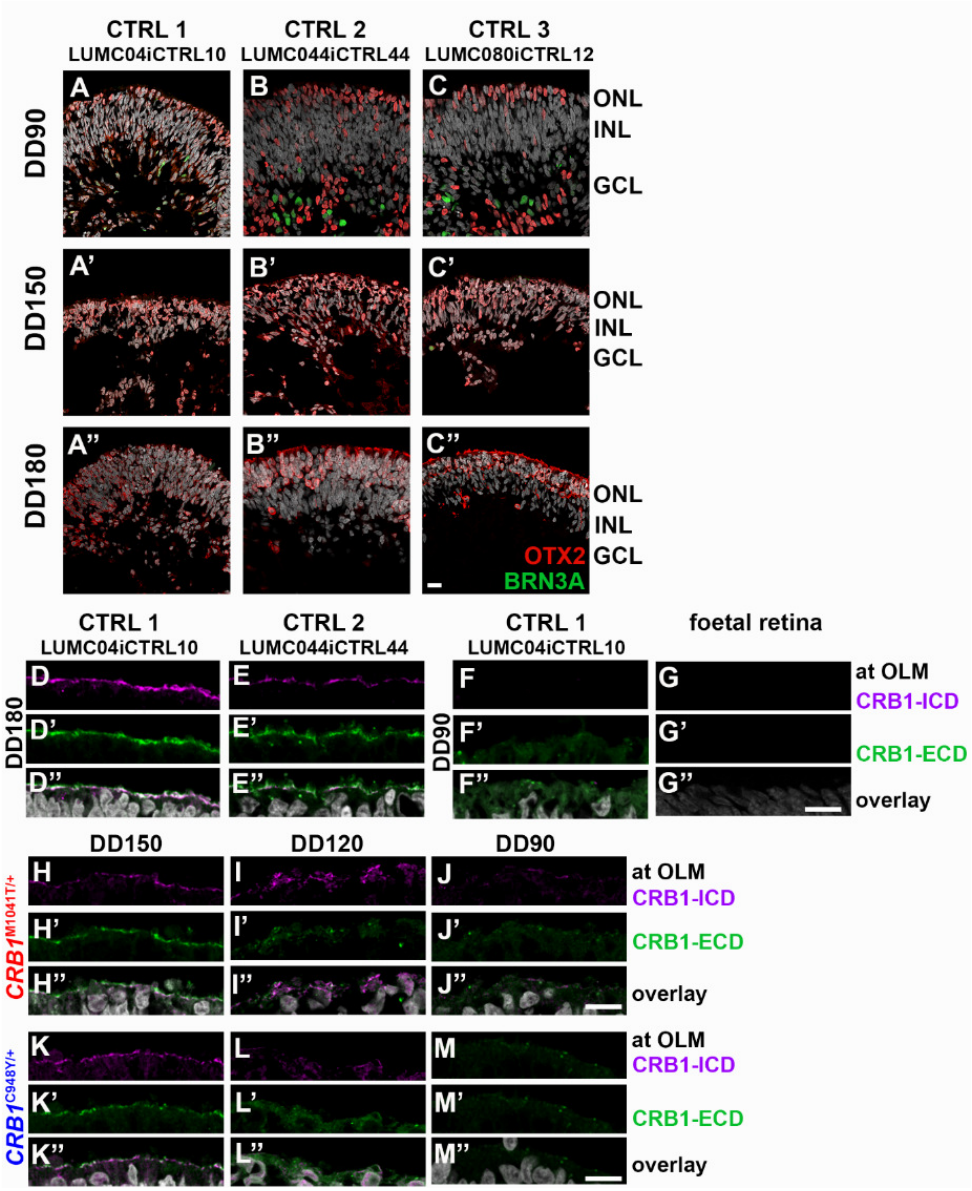

Figure S4. The onset of *CRB1* expression of CRB1 at >DD120 coincides with a well-defined ONL layer. Related to Figure 2. (A-C) Nuclei stained for OTX2 (early photoreceptor cells) and BRN3A (Ganglion cells; scale bar, 50 µm). (A-C) control organoids of three independent donors at DD90 (A-C), DD150 (A'-C'), DD180 (A''-C''). (D-M) CRB1 stained with an (D-M) intracellular (ICD) or (D'-M') extracellular domain (ECD) epitope antibodies at the OLM, and (D''-M'') overlay (scale bar, 10 µm) at DD180 (D-E; CTRL 1+2), DD90 (F; CTRL 1), human retina foetal gastation week 19 (G), DD150 (H+K; isogenic 1+2), DD120 (I+L; isogenic 1+2), and DD90 (J+M; isogenic 1+2). CTRL 1, LUMC04iCTRL10; CTRL2, LUMC044iCTRL44; isogenic 1, *CRB1*$^{M1041T/+}$; isogenic 2, *CRB1*$^{C948Y/+}$; OLM, outer limiting membrane; ICD, intracellular domain; ECD, extracellular domain; DD, differentiation day.

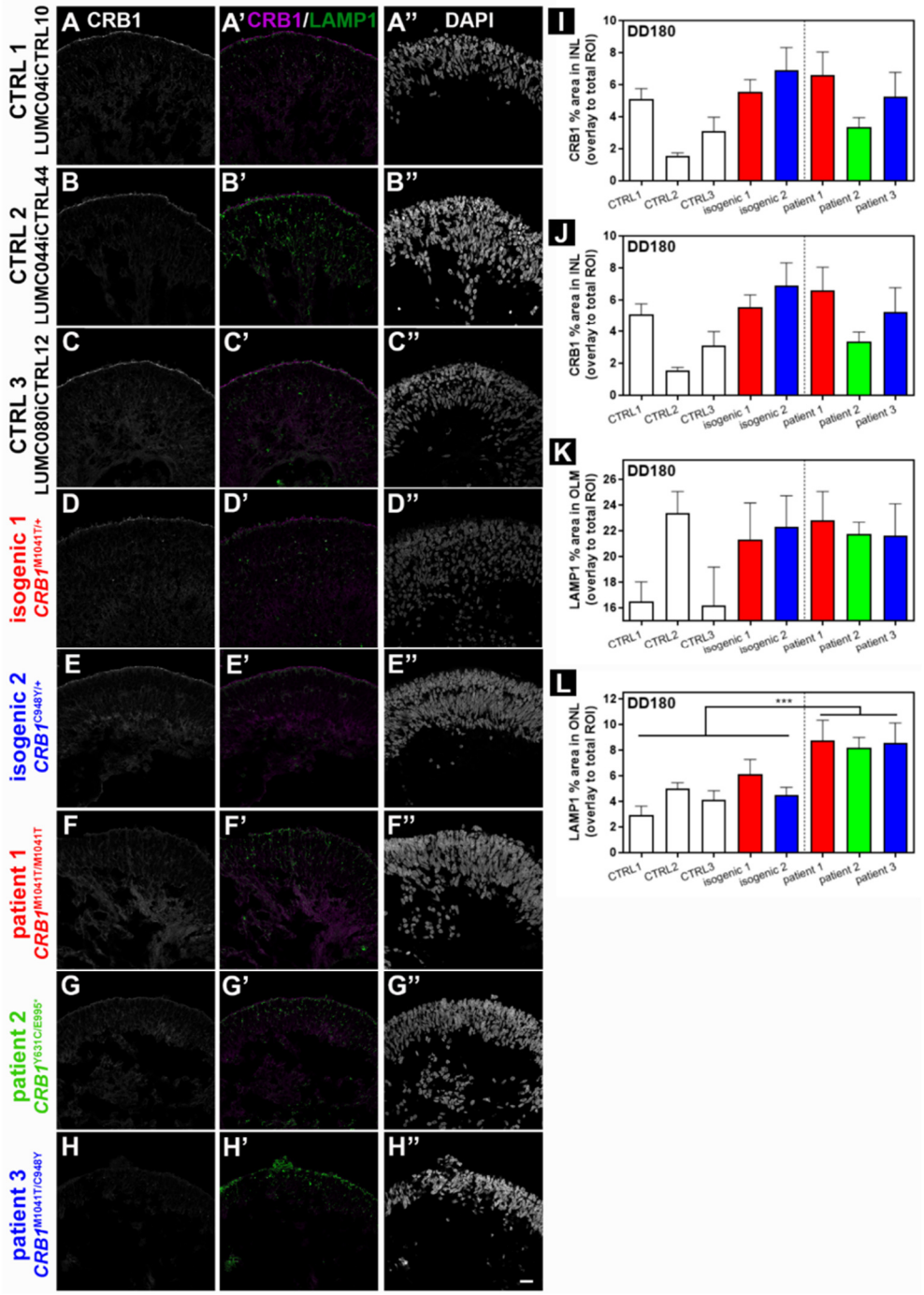
A CRB1
A' CRB1/LAMP1
A'' DAPI
CTRL 1 LUMC04iCTRL10
CTRL 2 LUMC044iCTRL44
CTRL 3 LUMC080iCTRL12
isogenic 1 CRB1M1041T/+
isogenic 2 CRB1C948Y/+
patient 1 CRB1M1041T/M1041T
patient 2 CRB1Y631C/E995*
patient 3 CRB1M1041T/C948Y
I
J
K
L
DD180
CRB1 % area in INL (overlay to total ROI)
LAMP1 % area in OLM (overlay to total ROI)
LAMP1 % area in ONL (overlay to total ROI)
***
CTRL1
CTRL2
CTRL3
isogenic 1
isogenic 2
patient 1
patient 2
patient 3

Figure S5. More lysosomes are present in *CRB1* patient retinal organoids. Related to Figure 4. Immunofluorescence CRB1 puncta (A-H; grayscale), co-labelling CRB1/LAMP1 (green/magenta in A'-H'), and nuclei (grayscale in A''-H'') in *CRB1* patient retinal organoids at DD180. (A-H) patient CRB1 retinal organoids express little CRB1 protein throughout the neuroretina. (A'-H') Little co-labelling of CRB1 (magenta) and lysosomes (LAMP1+, green) were found. (A'-H') Patient *CRB1* retinal organoids have more lysosomes at the ONL. (A''-H'') Nuclei staining (DAPI, grayscale) showing overall morphology. (I) CRB1-fluorescence signal measured by puncta in the INL. (I) The average CRB1 puncta size measured on fluorescence signal. (J-K) LAMP1+ puncta measured in the OLM and ONL. N=8-13 organoids per line. Scale bar, 50 µm.

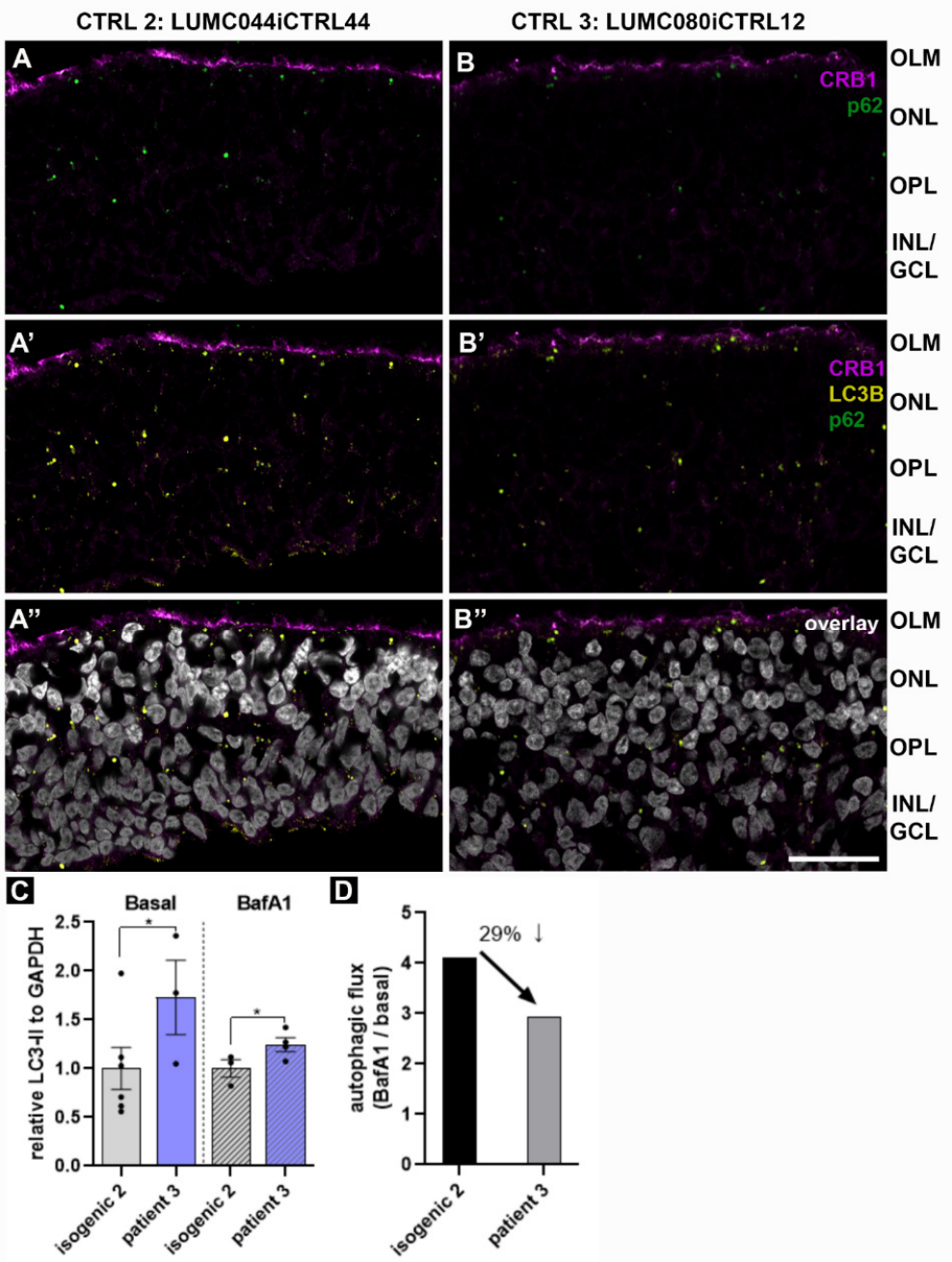
CTRL 2: LUMC044iCTRL44
CTRL 3: LUMC080iCTRL12
A
B
CRB1
p62
OLM
ONL
OPL
INL/
GCL
A'
B'
CRB1
LC3B
p62
A''
B''
overlay
C
Basal
BafA1
relative LC3-II to GAPDH
isogenic 2
patient 3
D
29% ↓
autophagic flux
(BafA1 / basal)

Figure S6. More degradative vesicles/compartments are present in *CRB1* patient retinal organoids. Related to Figure 5. (A-B) Immunofluorescence triple staining CRB1 (magenta), p62 (green), and LC3B (yellow). (A-B) LC3B and p62 localized overall more in OLM layer, OPL layer and INL layer in control retinal organoids. Scale bar, 50 µm. (C-D) Iso02-128 is the isogenic control line related to the patient 3 line (LUMC0128iCRB01, here called RP *CRB1*). (C) Analysis of the protein band intensities of the western blot shown in Figure 6I of individual lysed organoids (depicted as dots) stained for LC3B (LC3-I and LC3-II; 19/17 kD), recoverin for photoreceptors (26 kD), and GAPDH (housekeeping control, 37 kD) but organoids lacking recoverin expression were removed from the analysis. (D) Western blot protein band intensities of the BafA1 condition divided by the basal condition showing a decrease in the autophagic flux in *CRB1* patient retinal organoids.

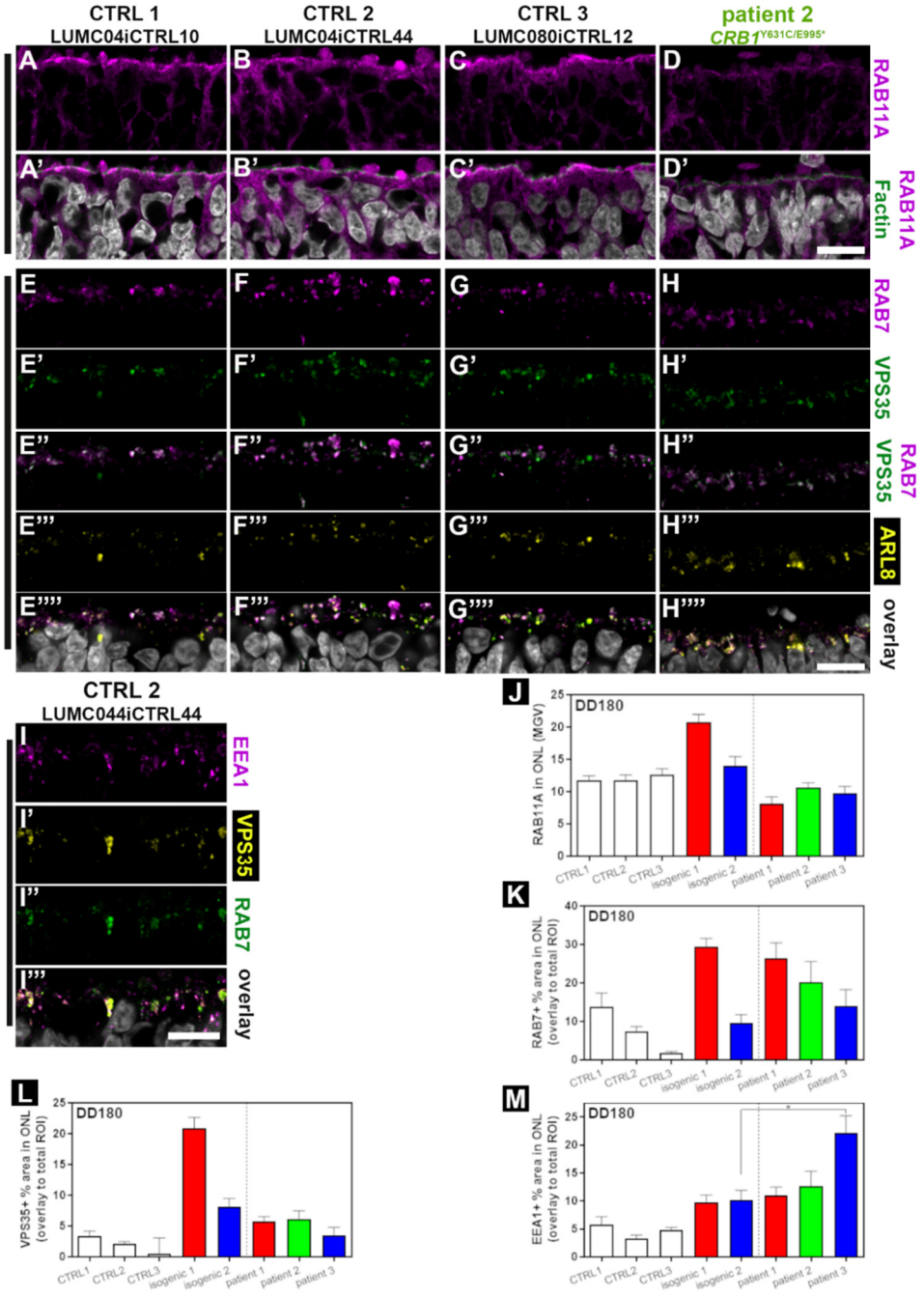
CTRL 1
LUMC04iCTRL10
CTRL 2
LUMC04iCTRL44
CTRL 3
LUMC080iCTRL12
patient 2
CRB1Y631C/E995*
RAB11A
RAB11A
Factin
RAB7
VPS35
RAB7
VPS35
ARL8
overlay
CTRL 2
LUMC044iCTRL44
EEA1
VPS35
RAB7
overlay
DD180
RAB11A in ONL (MGV)
DD180
RAB7+ % area in ONL (overlay to total ROI)
DD180
VPS35+ % area in ONL (overlay to total ROI)
DD180
EEA1+ % area in ONL (overlay to total ROI)
CTRL1
CTRL2
CTRL3
isogenic 1
isogenic 2
patient 1
patient 2
patient 3

Figure S7. Dysregulation of the endolysosomal system in patient *CRB1* patient retinal organoids. Related to Figure 7. (A+E) CTRL 1 (LUMC04CTRL10) retinal organoids, (B+F+I) CTRL 2 (LUMC044iCTRL44) retinal organoids, (C+G) CTRL3 (LUMC080iCTRL12) retinal organoids, and (D+H) patient 2 (LUMC0117iCRB01) retinal organoids. (A-D) Immunofluorescence labelling of RAB11A (magenta), and phalloidin (F-actin; green). (E-H) Immunofluorescence labeling of RAB7 (magenta), VPS35 (green), and ARL8A/B (yellow). (E-H) Immunofluorescence labeling of EEA1 (magenta), RAB7 (green), and ARL8A/B (yellow). (I) Immunofluorescence labeling of EEA1 (magenta), RAB7 (green), and VPS35 (yellow). Overlay shown in white (E-I). (J-M) Semi-quantification of fluorescence signal. (J) RAB11A mean gray value (MVG) in ONL. (K) Total RAB7 particle area / total ONL area in %. (L) RAB11A mean gray value (MVG) in ONL. (K) Total VPS35 particle area / total ONL area in %. (M) RAB11A mean gray value (MVG) in ONL. (K) Total EEA1 particle area / total ONL area in %. All retinal organoids at DD180 collected. Scale bar, 10 µm.

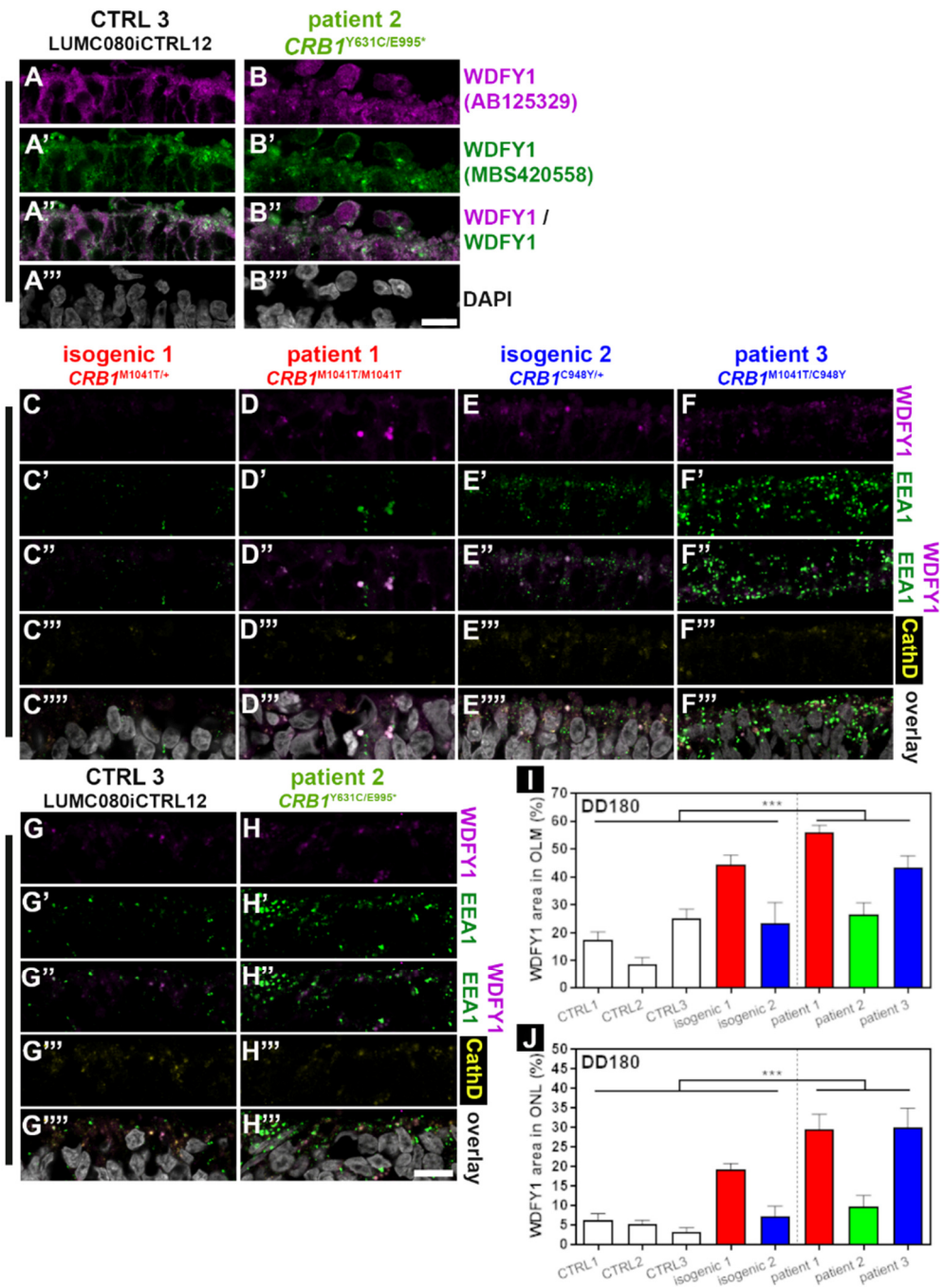
CTRL 3
LUMC080iCTRL12
patient 2
CRB1Y631C/E995*
A
B
WDFY1
(AB125329)
A'
B'
WDFY1
(MBS420558)
A''
B''
WDFY1 /
WDFY1
A'''
B'''
DAPI
isogenic 1
CRB1M1041T/+
patient 1
CRB1M1041T/M1041T
isogenic 2
CRB1C948Y/+
patient 3
CRB1M1041T/C948Y
C
D
E
F
WDFY1
C'
D'
E'
F'
EEA1
C''
D''
E''
F''
WDFY1
EEA1
C'''
D'''
E'''
F'''
CathD
C''''
D'''
E''''
F'''
overlay
CTRL 3
LUMC080iCTRL12
patient 2
CRB1Y631C/E995*
G
H
WDFY1
G'
H'
EEA1
G''
H''
WDFY1
EEA1
G'''
H'''
CathD
G''''
H'''
overlay
I
DD180
***
WDFY1 area in OLM (%)
0
10
20
30
40
50
60
70
CTRL1
CTRL2
CTRL3
isogenic 1
isogenic 2
patient 1
patient 2
patient 3
J
DD180
***
WDFY1 area in ONL (%)
0
5
10
15
20
25
30
35
40
45
50
CTRL1
CTRL2
CTRL3
isogenic 1
isogenic 2
patient 1
patient 2
patient 3

Figure S8. WDFY1 is more present in early endosomes in patient *CRB1* patient retinal organoids. Related to Figure 7. All organoids shown at DD180. (A-B) Immunofluorescence labelling of WDFY1 with two different antibodies (magenta / green) showing relative overlap. (C-H) Immunofluorescence labeling of WDFY1 (magenta; MBS420558 antibody), EEA1 (green), and Cathepsin D (yellow). Overlay shown in white (C-H). (I-J) Semi-quantification of fluorescence signal of WDFY1 (AB125329 antibody). (I) WDFY1 particle area / total OLM area in %. (J) WDFY1 particle area / total ONL area in %. CTRL3, wildtype line. Isogenic 1 and 2: isogenic control lines related to the patient line 1 (LUMC0116iCRB09) and patient line 3 (LUMC0128iCRB01). Scale bar, 10 µm.

Table S2: Antibody list and dilution used for immunohistochemistry and western blots. Related to all figures.

Host; antibody	Dilution + procedure	Catalogue number
Primary antibodies		
Mouse anti-CRB1-ECD	1/200 IF, 1/300 PLA	H00023418-A01
Rabbit anti-CRB1-ICD (AK2)	1/100 IF	Home-made
Phalloidin-TRITC (*aka* F-actin)	1/250 IF	r-415
Rabbit anti-OTX2	1/200 IF	13497-1-AP
Mouse anti-BRN3A	1/100 IF	sc-8429
Mouse anti-LC3B	1/100 IF + WB 1/300	0231-100/LC-3-5F10
Rabbit anti-FENS1	1/200 IF	AB125329
Mouse anti-EEA1	1/100 IF	BD-610457
Mouse anti-LAMP1	1/100 IF	sc-20011
Rabbit anti-Cathepsin D	1/200 IF	IM16-100UG
Mouse anti-ARL8A/B	1/100 IF	sc-398635
Mouse anti-NOTCH1-ECD	1/300 IF + PLA	MA5-11961
Mouse anti-PIP2	1/200 IF	MA3-500
Rabbit anti-(pan-)cytokeratin	1/200 IF	AB9377
Rabbit anti-RCVRN	1/600 IF, 1/5000 WB	AB5585
Mouse anti-GAPDH	1/5000 WB	MAB374
Rabbit anti-RAB7	1/100 IF	CST9367S
Goat anti-VPS35 (retromer)	1/100 IF	Ab10099
Rabbit anti-VPS26 (retromer)	1/250 IF	Ab181352
Rabbit anti-RAB11a	1/100 IF	71-5300
Rat anti-CD44	1/100 IF	553132
Mouse anti-Oct3/4-BV421	1/25 FACS	565644
Mouse anti-NANOG-PE	1/5 FACS	560483
anti-SSEA4-FITC	1/25 FACS	130-098-371
Mouse anti-Nestin-Alexa488 CC	1/200 IF	CST; clone 10C2
Rabbit PAX6-Alexa647 c CC	1/200 IF	CST; clone D3A9V
Rabbit FOXA2-Alexa555 CC	1/500 IF	CST; clone D56D6
Rabbit GATA4-Alexa647 CC	1/200 IF	CST; clone D3A3M
Rabbit Vimentin-Alexa647 CC	1/400 IF	CST; clone D21H3
Rabbit CDX2-Alexa555 CC	1/500 IF	CST; clone D11D10
Rabbit Brachyury-Alexa488 CC	1/200 IF	CST; clone D2Z3J
Secondary antibodies		
Anti-rabbit-IgG-HRP	1/5000 WB	sc-2357
Anti-mouse-IgGκ BP-HRP	1/5000 WB	sc-516102
Anti-rabbit Alexa647	1/1000 IF	Ab150083
Anti-mouse Alexa647	1/1000 IF	Ab150119
Anti-mouse Alexa488	1/1000 IF	Ab150113
Anti-chicken Alexa555	1/1000 IF	Ab150169
Anti-rabbit Alexa555	1/1000 IF	Ab150086
Anti-rat cy3 (50% glycerol added)	1/500 IF	712-165-153
Anti-rabbit cy3 (50% glycerol added)	1/500 IF	111-165-045

*IF, immunofluorescence; WB, western blot; PLA, Proximity ligation assay; CC, custom made conjugated

Table S3. RNAseq run-1. *Crb1*^{KO}*Crb2*$^{\Delta RPC}$ vs *Crb1*^{KO} at E15.5, E17.5, and P1.

(A) *Crb1*^{KO}*Crb2*$^{\Delta RPC}$ vs *Crb1*^{KO} : E15.5

	Symbol	Description	logFC	adj.P.val
	Upregulated			
1	Krt15	keratin 15	4,50	0,2
2	Abcd4	ATP-binding cassette, sub-family D, member 4	1,97	0,1
3	Col8a1	collagen, type VIII, alpha 1	1,85	0,3
4	9530091C08Rik	RIKEN cDNA 9530091C08 gene	1,69	0,2
5	Kcnq1ot1	KCNQ1 overlapping transcript 1	1,10	0,3
6	Fras1	Fraser extracellular matrix complex subunit 1	0,95	0,3
7	Col6a1	collagen, type VI, alpha 1	0,82	0,3
8	Zfp949	zinc finger protein 949	0,78	0,1
9	Dst	dystonin	0,53	0,2
10	Cacna1c	calcium channel, voltage-dependent, L type, alpha 1C subunit	0,48	0,3
	Downregulated			
1	Pax2	paired box 2	-2,16	0,2
2	Pcp4l1	Purkinje cell protein 4-like 1	-0,59	0,2
3	Mthfd2	methylenetetrahydrofolate dehydrogenase (NAD+ dependent), methenyltetrahydrofolate cyclohydrolase	-0,50	0,3
4	Cldn12	claudin 12	-0,41	0,3
5	Tnfrsf21	tumor necrosis factor receptor superfamily, member 21	-0,36	0,3
6	Tgfb2	transforming growth factor, beta 2	-0,36	0,2
7	BC023829	NA	-0,35	0,2
8	Pea15a	phosphoprotein enriched in astrocytes 15A	-0,34	0,2
9	Fzd5	frizzled class receptor 5	-0,32	0,3
10	Mxra7	matrix-remodelling associated 7	-0,32	0,3

***(B) Crb1*^{KO}*Crb2*$^{\Delta RPC}$ vs *Crb1*^{KO}: E17.5**

	Upregulated			
1	Abcd4	ATP-binding cassette, sub-family D (ALD), member 4	2,84	0,0
2	Cd68	CD68 antigen	0,80	0,2
3	Dmpk	dystrophia myotonica-protein kinase	0,75	0,1
4	Csf2ra	colony stimulating factor 2 receptor, alpha, low-affinity (granulocyte-macrophage)	0,74	0,2
5	Ryr3	ryanodine receptor 3	0,66	0,2
6	Pcdh15	protocadherin 15	0,64	0,2
7	Flrt1	fibronectin leucine rich transmembrane protein 1	0,62	0,1
8	Zfp949	zinc finger protein 949	0,61	0,2
9	Lime1	Lck interacting transmembrane adaptor 1	0,57	0,1
10	Pank4	pantothenate kinase 4	0,52	0,1

	Downregulated			
1	Slc7a3	solute carrier family 7 (cationic amino acid transporter, y+ system), member 3	-1,29	0,0
2	Chac1	ChaC, cation transport regulator 1	-1,13	0,2
3	Atf5	activating transcription factor 5	-0,97	0,0
4	Rhod	ras homolog family member D	-0,90	0,2
5	Morf4l1	mortality factor 4 like 1	-0,88	0,0
6	Slc7a5	solute carrier family 7 (cationic amino acid transporter, y+ system), member 5	-0,88	0,0
7	Sesn2	sestrin 2	-0,86	0,1
8	Ajuba	ajuba LIM protein	-0,73	0,2
9	Etv4	ets variant 4	-0,65	0,2
10	Cldn12	claudin 12	-0,62	0,0
	(C) *Crb1*^{KO}*Crb2*$^{\Delta RPC}$ vs *Crb1*^{KO}: P1			
	Upregulated			
1	Abcd4	ATP-binding cassette, sub-family D (ALD), member 4	1,84	0,1
2	Taf13	TATA-box binding protein associated factor 13	1,00	0,1
3	Zic1	zinc finger protein of the cerebellum 1	0,86	0,2
4	Dram2	DNA-damage regulated autophagy modulator 2	0,86	0,2
5	Atg3	autophagy related 3	0,79	0,2
6	Srsf5	serine/arginine-rich splicing factor 5	0,70	0,2
7	Zfp422	zinc finger protein 422	0,64	0,2
8	Lipt2	lipoyl(octanoyl) transferase 2 (putative)	0,63	0,2
9	Syt4	synaptotagmin IV	0,57	0,2
10	Klf10	Kruppel-like factor 10	0,57	0,2
	Downregulated			
1	Neurog2	neurogenin 2	-0,62	0,2
2	Zfp773	zinc finger protein 773	-0,59	0,2
3	Zfp790	zinc finger protein 790	-0,51	0,2
4	Armcx1	armadillo repeat containing, X-linked 1	-0,49	0,2
5	Reck	reversion-inducing-cysteine-rich protein with kazal motifs	-0,48	0,2
6	Rnf6	ring finger protein (C3H2C3 type) 6	-0,45	0,2
7	Parp11	poly (ADP-ribose) polymerase family, member 11	-0,45	0,2
8	Amotl2	angiomotin-like 2	-0,44	0,2
9	Cln8	ceroid-lipofuscinosis, neuronal 8	-0,44	0,2
10	Cntrl	centriolin	-0,42	0,1

Table S4. RNAseq run-2. *Crb1*^{KO}*Crb2*$^{\Delta RPC}$ vs wildtype control at E15.5

	Symbol	Description	logFC	adj.P.Val
	Upregulated			
1	Gja8	gap junction protein, alpha 8	4,14	0,18
2	Igfbp7	insulin-like growth factor binding protein 7	3,43	0,21
3	Synpr	synaptoporin	2,75	0,00
4	Abcd4	ATP-binding cassette, sub-family D (ALD), member 4	2,50	0,00
5	Wdfy1	WD repeat and FYVE domain containing 1	2,47	0,00
6	Gfi1	growth factor independent 1	2,26	0,00
7	Tbx20	T-box 20	2,11	0,00
8	Chrnb3	cholinergic receptor, nicotinic, beta polypeptide 3	2,04	0,00
9	Sparcl1	SPARC-like 1	1,96	0,00
10	Sptb	spectrin beta, erythrocytic	1,93	0,00
	Downregulated			
1	Tmem181b-ps	transmembrane protein 181B, pseudogene	-4,83	0,00
2	Crb1	crumbs family member 1, photoreceptor morphogenesis associated	-4,15	0,00
3	Snca	synuclein, alpha	-3,91	0,00
4	Dusp9	dual specificity phosphatase 9	-2,12	0,00
5	Grm2	glutamate receptor, metabotropic 2	-2,10	0,00
6	Capn6	calpain 6	-1,88	0,19
7	Sfrp2	secreted frizzled-related protein 2	-1,62	0,00
8	Crabp1	cellular retinoic acid binding protein I	-1,47	0,00
9	Gpnmb	glycoprotein (transmembrane) nmb	-1,46	0,08
10	Sst	somatostatin	-1,33	0,18